The northward meridional flow into the South Atlantic, the South Pacific, and the Indian Oceans

Doron Nof

Department of Oceanography 4320

The Florida State University

Tallahassee, Florida 32306-4320 U.S.A.

nof@ocean.fsu.edu

* *Also affiliated with The Geophysical Fluid Dynamics Institute, Florida State University*

Revised, August 2002

Abstract

Recently, a "quasi-island" approach for examining the meridional flux of warm and intermediate water from the Southern Ocean into the South Atlantic, the South Pacific and the Indian Ocean was proposed (Nof 2000a, 2002). The method considers the continents to be "pseudo islands" in the sense that they are entirely surrounded by water but have no circulation around them. The method employs an integration of the linearized momentum equations along a closed contour containing the continents. This allows one to compute the meridional transport into these oceans without finding the detailed solution to the complete wind-thermohaline problem.

The solution gives one expected and one unexpected result. It shows that, as expected, about 9 ± 5 Sv of upper and intermediate water enter the South Atlantic from the Southern Ocean. It also shows, however, the unexpected result that the Pacific-Indian Ocean system should contain a "shallow" meridional overturning cell carrying 18 ± 5 Sv. By "shallow" it is meant here that the cell does not extend all the way to the bottom (as it does in the Atlantic) but is terminated at mid-depth. (This reflects the fact that there is no bottom water formation in the Pacific.) Both of these calculations rely on the observation that there is almost no flow through the Bering Strait and on the assumption that there is a negligible pressure torque on the Bering Strait's sill.

Here, we present a new and different approach which does not rely on the above two conditions regarding the Bering Strait and yet gives essentially the same result. The approach does not involve any quasi-island calculation but rather employs an integration of the linearized zonal momentum equation along a closed open-water latitudinal belt connecting the tips of South Africa and South America. The integration relies on the existence of a belt (corridor) where the linearized general circulation equations are valid. It allows for a net northward mass flux through either the Sverdrup interior or the western boundary currents. It is found that the belt-corridor approach gives 29 ± 5 Sv for the total meridional flux of surface and intermediate water from the Southern Ocean. This agrees very well with the above-mentioned quasi-island calculations which give a total northward flux of 27 ± 5 Sv. Given the spacing between the continents and the small variability of the southern winds with longitude, one may assume that out of the 29 Sv, 9 Sv enter the Atlantic and 20 Sv enter the combined Pacific-Indian Ocean system which is also in agreement with the quasi-island calculation. These agreements indicate that the assumptions made in the earlier studies regarding the Bering Strait are probably valid.

Keywords: Ocean currents, Western Boundary Currents, meridional flow, Southern Ocean

1. Introduction

The Southern Ocean constitutes the most important geographic asymmetry in the world ocean because it provides a free communication between the Atlantic, the Pacific and the Indian Ocean. Encompassing the entire globe, it is subject to very strong winds which drive both zonal and meridional flows. We shall demonstrate in this article that this geographic asymmetry is crucial to the meridional flow in the world ocean.

1.1. Overview

Much has been written on the Antarctic Circumpolar Current (ACC) and the manner by which the energy input by the wind is dissipated (see e.g., Munk and Palmen, 1951; Clarke, 1982; Nowlin and Klinck, 1986; Johnson and Bryden, 1989; Treguier and McWilliams, 1990; Killworth, 1991; Straub, 1993; Killworth and Nanneh, 1994; Marshall, 1995; Ivchenko et al., 1996; Krupitsky et al., 1996; Gille, 1997; Stevens and Ivchenko, 1997; and Tansley and Marshall, 2001a,b). Attention has also been given to the relationship between the ACC and the connection of the Southern Ocean with rectangular basins closed on the northern side (see e.g., Kamenkovich, 1962; and Gill and Bryan, 1971). Such models do not allow for net "conveyor" transports or deep water formation in the northern hemisphere and are, therefore, of limited importance to the problem posed in this study.

Here, we do not focus on the ACC but rather on the net inter-hemispheric northward flux through the region immediately to the *north* of the ACC, where the three lower-latitude oceans (Atlantic, Pacific and Indian) meet the Southern Ocean. This boundary separating the Southern Ocean from the lower-latitude oceans can be thought of as a narrow closed contour connecting the southern tip of the Americas with the southern tip of Africa and the southern tip of New Zealand (**Fig. 1**). Using an analytical model we shall show that, in line with the recent quasi-island models (Nof 2000a, 2002), the northward transport of upper and intermediate water across this contour (or a "belt") is driven into the lower-latitude oceans solely by the *wind field.* **Fig. 2** displays the flow field associated with one of these quasi-island calculations.

Before describing the details of our calculations, it is appropriate to point out that, although this particular aspect of the northward meridional transport has not been addressed before, the

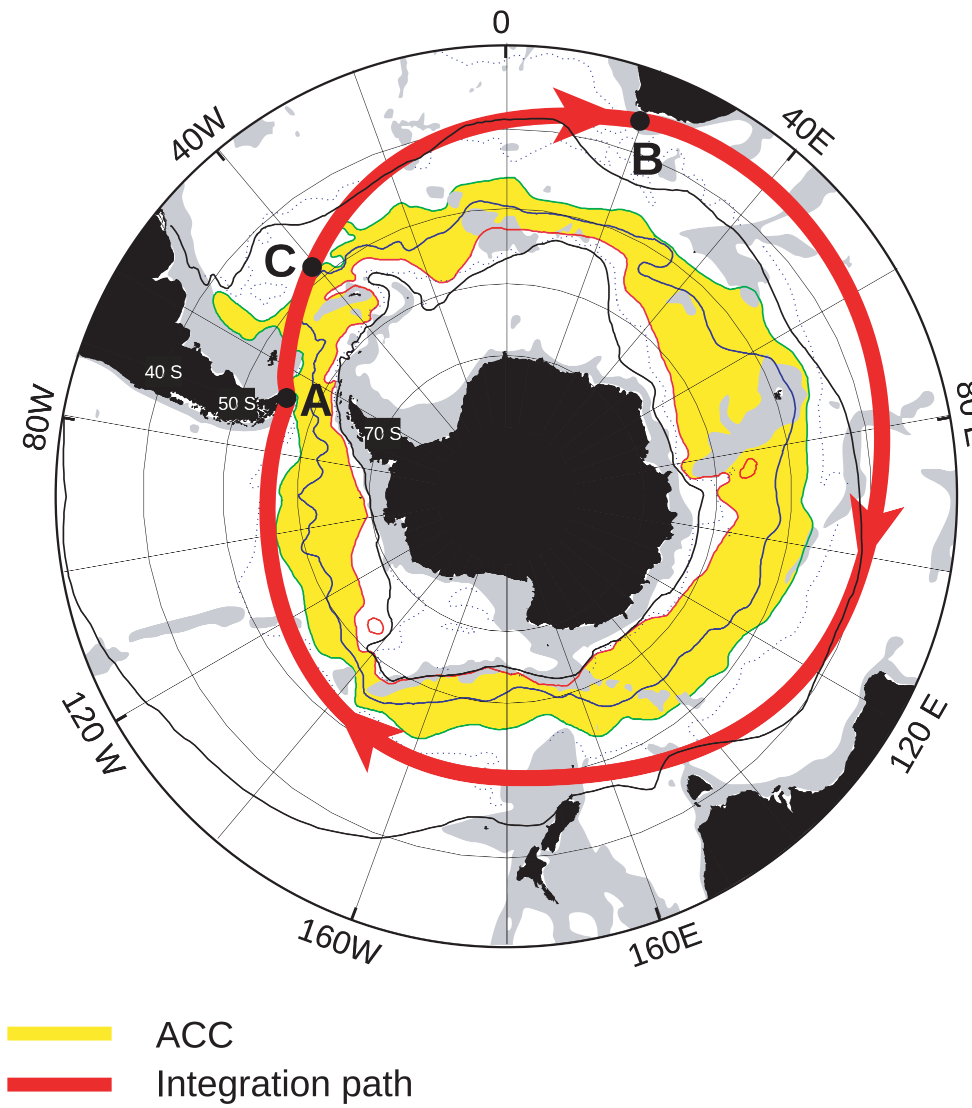

Fig. 1. A diagram of the mean ACC position (yellow, adapted from Orsi et al., 1995) and the closed integration path (thick red contour) used in the realistic analytical belt model. The integration is done mainly in the zonal direction. Note that the contour consists of the

two southernmost boundaries of the contours already used in the earlier quasi-island calculations (Nof 2000, 2002) . Also, note that the integration path is, by and large, outside the ACC. The only section where the integration path crosses the ACC (and the momentum balance used to derive our transport formula is violated) is the Drake Passage and its immediate vicinity (AC). Since this section is small compared to the entire integration path, and, since the actual form-drag exerted by the Drake Passage on the ACC is no more than 15-20% of the entire ACC bottom drag (see e.g., Gille, 1997), the error introduced by this crossing (of the ACC) is small. Finally, note that there is very little room between the southern tips of the continents and the northern edge of the ACC to fit the integration contour. This implies that the sensitivity of the computed transport to the particular choice of the integration path (and its associated wind dependency) is minimal.

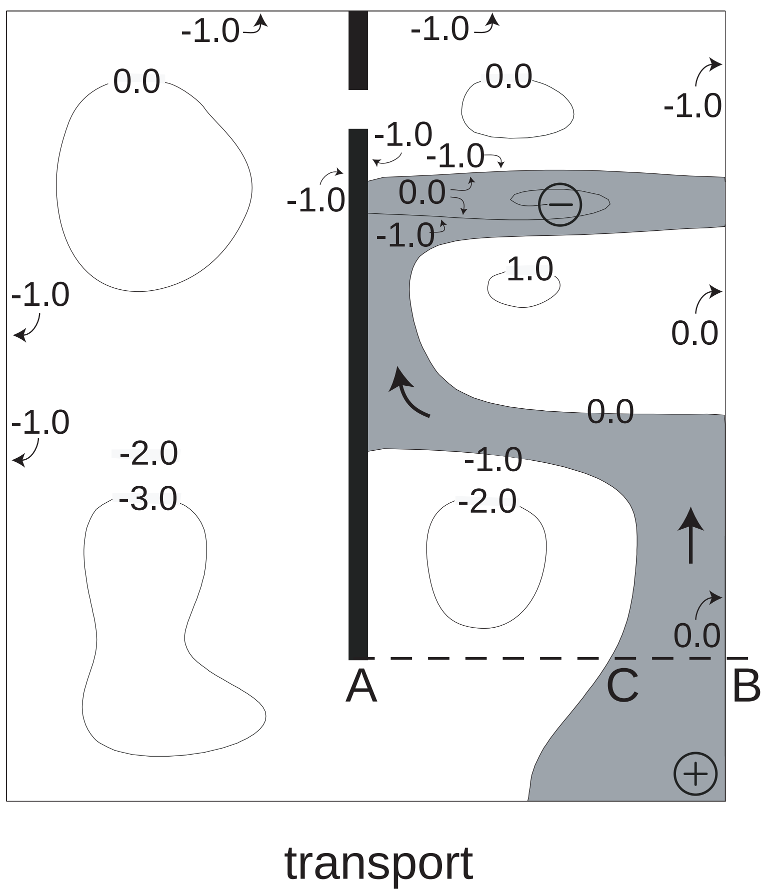

Fig. 2. Nondimensional transport contours for the quasi-island Atlantic simulation (Nof 2000a) with a northern gap (Bering Strait). The source and sink accommodate the transport (across AB) required by the wind. (Here, the sink is situated in the middle of the ocean and, consequently, there is a discontinuity in the transport function along both the island and the eastern boundary.) Shaded region indicates the meridional overturning cell (MOC). Note that across AB the MOC constitutes the Sverdrup flow along the eastern part of the basin (CB). This vividly illustrates that much of the Ekman flux across the South Atlantic (AC) does not end up in the northern hemisphere and is, therefore, not a part of the MOC. This Ekman flux (i.e., the flux through AC) is simply flushed out of the basins after entering it. Reproduced from Nof (2000a).

closely related (shallow) Deacon (and other) cells connecting the Southern Ocean with the lower-latitude oceans has been dealt with. Most of these studies were either entirely numerical (Manabe et al. 1990; Döös 1994) or quasi-analytical (Döös 1994). Although they are informative, they do not directly address the issue of how important is the wind field compared to the thermohaline circulation nor do they deal with the issue of the total net northward transport.

1.2. Approach

Our approach involves integration of the linearized vertically integrated momentum equations along a closed contour which is *just outside the ACC* and yet not far enough north to be inside the lower latitude oceans (**Fig. 1**). There is a very narrow latitudinal corridor along which both of these conditions are satisfied. It is no more than a few hundred kilometers broad and the wind does not vary much across it. The closed contour passes through the tips of the Americas, Africa and Australia. Since it is situated outside the ACC, the associated fluid is subject to Sverdrup dynamics and dissipative western boundary currents (created by the presence of the continents). It does not involve, however, zonal friction, eddy fluxes, and form-drag processes which are important to the ACC. Consequently, the vertically integrated *zonal* momentum equation does not involve friction and its pressure term drops out upon integration along the closed contour (which, as alluded to earlier, passes in its entirely through open water). This provides a direct relationship between the integrated wind stress and the meridional transport. In a way, this approach is similar to the traditional island calculation of Godfrey (1989), Pedlosky et al. (1997) and Pratt and Pedlosky (1998) except that the "island" is now Antarctica.

Consider first the idealized ocean shown in **Fig. 3**. This simplified configuration (hereafter referred to as the "first analytical model") is sufficient for illustrating the essence of the problem and is used here merely for the clarity of the presentation. Actual analytical calculations will be done with the more realistic geography shown earlier in **Fig. 1**. We shall consider first the familiar vertically integrated equations of motion corresponding to an ocean north of the ACC. The interior obeys Sverdrup dynamics and dissipation occurs underneath the swift WBC as a result of

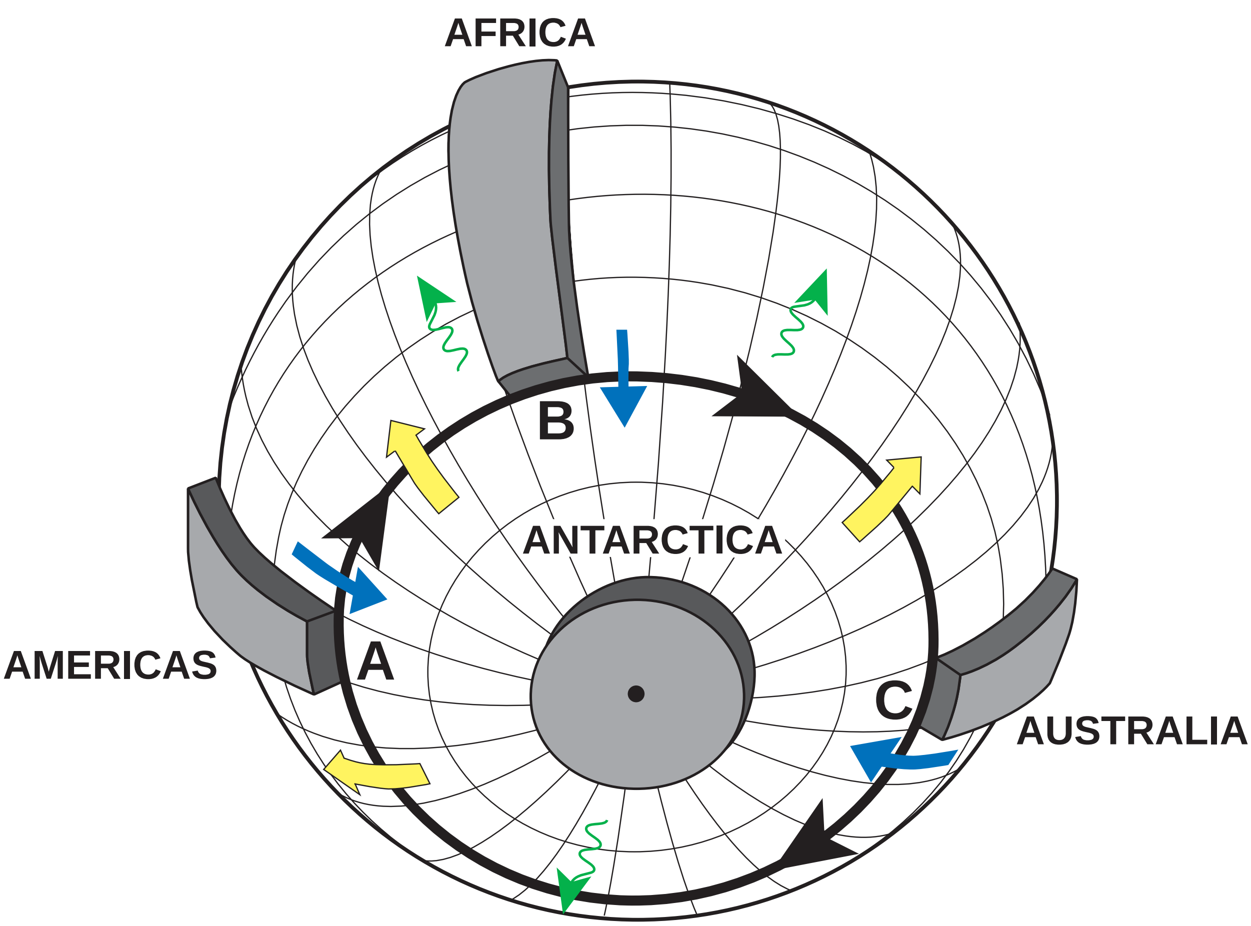

Fig. 3a. Schematic diagram of the simplified geography used in our first analytical model. The integration is done along a latitudinal circle passing through the southern tips of the continents (represented by the three peninsulas). The integration contour is situated inside a latitudinal corridor just outside the ACC where the familiar linearized equations of motion are valid. Green "wiggly" arrows denote the net meridional mass flux. This net flow is a result of the manner by which the WBC (narrow blue arrows) and the Sverdrup interior (thick yellow arrows) combine.

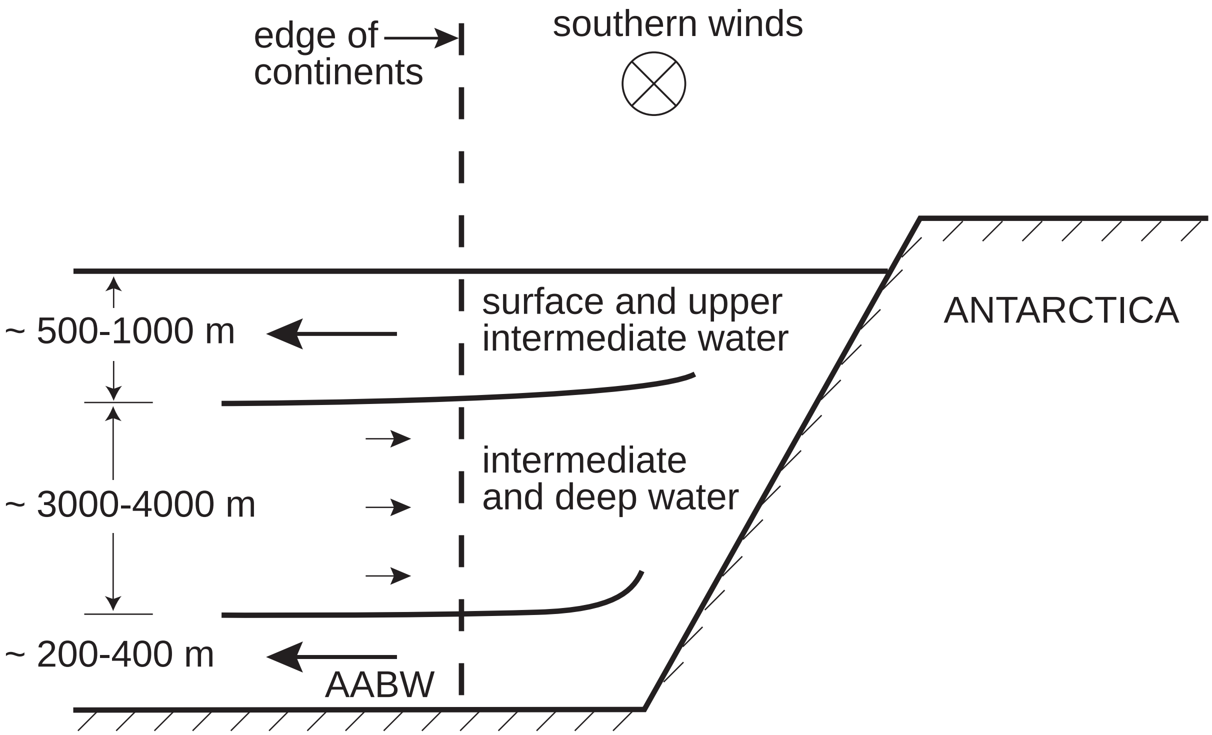

Fig. 3b. A schematic longitudinal cross section of our model. The dashed line indicates the edge of the continents. The surface and upper intermediate water flows northward in the continuously stratified shallow upper layer (~500-1000 m thick). This shallow active layer overlies a very thick (~3000-4000 m) layer whose speeds (but not necessarily the transports) are small and negligible. A third deep layer (not shown) that carries deep water (such as the NADW) flows southward (as a western boundary current leaning against the ridges) underneath the very thick intermediate water. AABW [O(100 m) thick] is also flowing along the floor. As earlier works have indicated, both the southward flowing deep water (not shown) and the northward flowing AABW require deep meridional walls in order to exist. Neither one of these waters is presented explicitly in our model and, consequently, we do not include meridional walls in our model.

interfacial friction. As before, some nonlinearity is contained in the model through the pressure terms (which allow large vertical displacement of the interface) but the inertial terms are neglected.

As in the quasi-island calculations, the common demand that, in a closed basin, the WBC transport be equal and opposite to that of the interior is relaxed so that a net meridional flow out of the region of interest is allowed. Such a net transport is, in general, a result of a combined interior and WBC fluxes. With the aid of these considerations, and an integration along a closed path connecting the tips of the continents, we shall analytically derive a formula that allows the computation of the meridional transport from the wind field. We shall see that this meridional transport includes flows due to *both wind and diabatic* processes even though the thermodynamics enter the problem implicitly and not explicitly. This follows from the Boussinesq approximation which implies that the interior transport is not affected by the density.

The above scenario involves the implicit assumption that the ocean is in a steady state implying that either the net upper ocean meridional transport across the contour shown in **Fig. 3** is zero or that whatever is transported northward is removed via deep water formation, atmospheric cooling, or diapycnal mixing. Any upper water northward transport must ultimately come back to the Southern Ocean as deep southward boundary currents along the flanks of the meridional ridges connecting the Antarctic continent to the Pacific, Indian and Atlantic basins.

After presenting the transport formula for the first analytical model and illustrating the essence of the problem (Section 2), we shall proceed and extend the transport formula to the more realistic second analytical model shown earlier in **Fig. 1**. In this latter context, we shall include the following: (i) meridional winds; (ii) the sphericity of the earth; and (iii) the actual geometry of the boundaries. This is followed by presenting process-oriented numerical experiments (Section 3) and comparing them to our transport formula for the simplified ocean (the first analytical model). Some discussion of the results is included throughout the presentation; the application to the Atlantic, Pacific and Indian Oceans is presented in detail in Section 4. Section 5 includes a clarification of the northward mass flux and its relationship to the Ekman flux. A summary is given in Section 6.

2. The new analytical model

2.1. Governing equations

Consider again our first model (**Fig. 3**). The conceptual model contains four layers. An upper, continuously stratified, northward flowing layer contains the Ekman flow, the geostrophic flow underneath and the western boundary current. It is anywhere from 500 m to 1000 m thick where a level of no motion is assumed. The level-of-no-motion assumption coincides with a density surface but its depth varies in the field. Below this level the density is assumed to be constant. The upper moving layer contains both thermocline and some intermediate water, as some intermediate water is situated above the level of no motion. It is continuously stratified [$\rho = \rho(x,y,z)$] and is subject to both zonal wind action and heat exchange with the atmosphere. Underneath this active layer there is a very thick (3000–4000 m) intermediate layer whose speeds [but not necessarily the transports (see e.g., Gill and Schumann, 1979)] are small and negligible. Underneath this thick layer there are two active layers which are not explicitly included in the model and require a meridional wall to lean against. The first is the southward flowing layer which carries water such as the NADW; it is ~O(1000 m) thick. The second is the AABW layer whose thickness is ~O(100 m). The level-of-no-motion assumption in high latitudes is potentially problematic (see e.g., Peterson 1992) but its limitations with regard to the latitudes that we use here were already discussed at length in Section 1b of Nof (2002) and need not be repeated here.

The familiar linearized Boussinesq equations for the upper layer are,

$$-fv = -\frac{1}{\rho_0}\frac{\partial P}{\partial x} + \frac{1}{\rho_0}\frac{\partial \tau^x}{\partial z} \tag{2.1}$$

$$fu = -\frac{1}{\rho_0}\frac{\partial P}{\partial y} + \frac{1}{\rho_0}\frac{\partial \tau^y}{\partial z} \tag{2.2}$$

$$g = -\frac{1}{\rho}\frac{\partial P}{\partial z} \tag{2.3}$$

$$\frac{\partial u}{\partial x} + \frac{\partial v}{\partial y} + \frac{\partial w}{\partial z} = 0 \quad , \tag{2.4}$$

where *u, v* and *w* are the velocities in the *x, y* and *z* directions (here, *x* is pointing eastward and *y* is pointing northward), *f* is the Coriolis parameter (varying linearly with *y*), ρ_0 the uniform density of the motionless deep water, ρ the moving layer density [$\rho = \rho(x, y, z)$], *P* is the deviation of the hydrostatic pressure from the pressure associated with a state of rest, τ^x is the stress in the *x* direction and τ^y is the meridional stress. Friction will only be included in the *y* momentum equation on the ground that it will only be important within the WBC. Our numerical simulation will later support this assumption.

Next, we define a vertically integrated pressure anomaly,

$$P^* = \int_{-\xi}^{\eta} P dz \quad , \tag{2.5}$$

where ξ(x,y) is the depth of the level of no horizontal pressure gradient (say, 1500 m) and η is the free surface vertical displacement. Using Leibniz's formula for the differentiation under the integral,

$$\frac{\partial P^*}{\partial x} = \int_{-\xi}^{\eta} \frac{\partial P}{\partial x}\, dz + P(\eta)\frac{\partial \eta}{\partial x} - P(-\xi)\frac{\partial \xi}{\partial x},$$

one can show that

$$\frac{\partial P^*}{\partial x} = \int_{-\xi}^{\eta} \frac{\partial P}{\partial x}\, dz \quad and \quad \frac{\partial P^*}{\partial y} = \int_{-\xi}^{\eta} \frac{\partial P}{\partial y}\, dz\ , \tag{2.6}$$

because $P = 0$ at $z = -\xi$ and $P(\eta)\dfrac{\partial \eta}{\partial x}$ is negligible by virtue of the rigid lid approximation. Using (2.6), vertical integration of (2.1 – 2.3) from $-\xi$ to η gives,

$$-fV = -\frac{1}{\rho_0}\frac{\partial P^*}{\partial x} + \frac{\tau^x}{\rho_0} \tag{2.7}$$

$$fU = -\frac{1}{\rho_0}\frac{\partial P^*}{\partial y} - RV \tag{2.8}$$

$$\frac{\partial U}{\partial x} + \frac{\partial V}{\partial y} = 0 \quad , \tag{2.9}$$

where U and V are the vertically integrated transports in the x and y directions, and R is an interfacial friction coefficient which, as we shall see, need not be specified for the purpose of our analysis. The analogous term RU does not appear in (2.7) because our region of interest is out of the ACC so that U is small. The equations are valid for all latitudes including the equator. Elimination of the pressure terms between (2.7) and (2.8) and consideration of (2.9) gives,

$$\beta V = -\frac{1}{\rho_0}\frac{\check{Z}\tau^x}{\partial y} - R\frac{\partial V}{\partial x} \quad , \tag{2.10}$$

which, for the inviscid ocean interior, reduces to the familiar Sverdrup relationship,

$$\beta V = -\frac{1}{\rho_0}\frac{\check{Z}\,\tau^x}{\partial y} \quad , \tag{2.11}$$

Six comments should be made with regard to (2.7 – 2.11):

i. Thermohaline effects enter the equations through the deviation of the hydrostatic pressure from the pressure associated with a state of rest which is represented in P^*.

ii. Energy is supplied by both the wind and cooling; dissipation occurs through interfacial friction [i.e., the RV term in (2.8)] within the limits of the WBC system. Interfacial friction is not present in (2.7) because we assume that RU is small and negligible. Furthermore, since the velocities are small in the ocean interior the frictional term is taken to be negligible there.

iii. Relation (2.7) holds both in the sluggish interior away from the boundaries and in the intense WBC where the flow is geostrophic in the cross-stream direction. Within the WBC the balance is between the Coriolis and pressure terms with the wind stress playing a secondary role. In the interior, on the other hand, the velocities are small and, consequently, all three terms are of the same order.

iv. The inertial terms are excluded from the model but nonlinearity is included in the pressure terms in the sense that the pressure deviations from a state of rest can be large. Since the model does not include relative vorticity within the WBC, it implicitly assumes that all the relative vorticity generated by moving the fluid meridionally (within the boundary layer) is dissipated immediately after its creation. (This implies that cross-equatorial flows can easily take place via the WBC where the fluid does not "remember" its origin.)

v. The frictional coefficient determines the width of the WBC but not its length (which, in turn, is controlled by the wind field and the pressure along the eastern boundary). In other words, the WBC adjusts its width in such a way that the total energy input (by the wind) is always dissipated along its base.

vi. Since *there is a net meridional flow* in our model, the WBC transport is not equal and opposite to that of the Sverdup interior to its east. Furthermore, since the Sverdrup transport is fixed for a given wind field, it is the WBC that adjusts its transport to accommodate the net meridional transport imposed on the basin.

vii. In our scenario the Sverdrup transport is applied only to the fluid above the level-of-no-motion (even though the Sverdrup transport can be applied to the entire fluid column from top to bottom). Namely, the interior transport below the level-of-no-motion is neglected. This is not necessarily the case with the WBC where the transport underneath the level of no motion can still be important. This is so because, although the velocities are required to be small there, the thickness is large so that the transport can be of O(1) without violating the level-of-no-motion assumption. A thin deep returning flow of a greater density is, of course, also allowed. The vertical velocity w is negligible along the integration contour but is not necessarily zero elsewhere in the field.

2.2. Integration of the momentum equation

To derive the transport formula for the first analytical model, we integrate (2.7) along the enclosed latitudinal circle shown in **Fig. 3**. Since the integral of the pressure term is identically zero, we immediately get,

$$-f_0 T = \oint \left(\frac{\tau^x}{\rho_0} \right) dx \quad , \tag{2.12}$$

where T is the net meridional transport across the ocean and f_0 is the Coriolis parameter along the contour. This is our desired formula for the first simplified analytical belt model. Note that, even though (2.12) looks like the familiar Ekman transport, it includes the Ekman flow, the geostrophic flow underneath and the transport of the WBC because both the equation and the region that we integrated across include those features. Namely, (2.12) looks like the Ekman flux but addresses a different water mass than the classical Ekman flux does; this is because the WBC transport cancels the geostrophic transport in the interior so that the total transport is identical to the amount given by the Ekman transport. Just as is shown in **Fig. 2** [adapted from Nof's (2000a) calculation], this implies that the waters entering the northern oceans do so via the Sverdrup interior along the eastern parts of the basins rather than via the Ekman layer. Much of the northward Ekman transport across our contour (**Fig. 3a**) is flushed out of the South Atlantic and South Pacific–Indian system via the recirculating gyres. This subtle point is discussed in detail in Section 5.

Relation (2.12) gives the combined (wind and cooling) transport in terms of the wind field and the geography alone. This means that cooling controls the local dynamics (i.e., where and how the sinking occurs as well as the total amount of downwelling and upwelling) but does not directly control the net amount of water that enters the South Atlantic, the South Pacific and the Indian Ocean. We shall return to this important point momentarily. As mentioned earlier, (2.12) can only be applied to a latitudinal belt "kissing" the tips of the continents. Away from the tips the ACC is established and the RU term in (2.7) representing form drag, friction, and eddy fluxes is no longer negligible. Equation (2.12) may give the erroneous impression that, due to Stokes' theorem, it simply corresponds to an integration of the wind stress curl (and, hence, the Sverdrup interior) over the area. This is not the case as the conversion of surface to line integral does not make any sense here because a large portion of the area is land (Antarctica) where the equations do not hold.

2.3. Properties of the new transport formula

In this section we shall describe several properties of (2.12) and extend it to more general cases involving meridional winds and more complex geography.

2.3.1. The limits

As mentioned, the expression for the meridional transport (2.12) does not contain any cooling *explicitly* because explicit cooling enters the problem only through the density which, with the Boussinesq approximation, does not affect our transport. We also note that, according to (2.12), in the absence of wind there can be no net meridional flow into the Atlantic, Pacific and Indian Oceans even if there is asymmetrical high-latitude cooling in these oceans. This implies that without winds, whatever sinks or upwells in these oceans must be compensated for by upwelling (or downwelling) somewhere else within the confines of these oceans. As mentioned, this does not necessarily imply that the wind directly determines the amount of water sinking in the North Atlantic or the Pacific but it does imply that sinking in general is accompanied by at least a partially compensating upwelling (elsewhere within the limits of these oceans). In this scenario the wind controls the *net* amount that is drawn from the Southern Ocean into the lower latitude oceans.

As in Nof's (2000a, 2002) quasi-island situations, these properties can be summarized as follow:

1. In the limit of no wind ($\tau^x \equiv 0$), no water can get in and out of the lower latitude oceans and whatever sinks in them has to upwell elsewhere within their boundaries.
2. In the limit of no NADW, an Atlantic MOC will still exist but it will not extend over the entire water column [i.e., it will constitute a shallow MOC as is presently the case in the Pacific (Nof 2002)].

2.3.2. Extension of the formula to a "realistic" analytical model

It is a simple matter to extend the results of the first continuously stratified model to a more realistic model containing meridional winds and a bit more complicated geometry (**Fig. 1**). As mentioned, we shall refer to this more realistic model as the "second analytical model." Using again the Boussinesq approximation and the vertically integrated equations in spherical coordinates, one ultimately arrives at the formula (2.1),

$$T = \oint -\frac{\tau^{\ell} d\ell}{f_{\ell}\rho_0} \quad , \tag{2.13}$$

where T is the total transport, f_{ℓ} the *average* Coriolis parameter along the contour shown in **Fig. 1**, and ℓ indicates the component *along* the closed integration path. It is important to realize that (i) by taking the Coriolis parameter to be a constant along the belt (**Fig. 1**) we introduced an error of 15–20% because this is how much f varies across the actual contour; and (ii) the wind hardly varies across the corridor that (2.13) can be applied to.

2.3.3. Potential frictional and eddy fluxes effects

When interior frictional effects and zonal stresses associated with zonal current (such as the ACC) or eddy fluxes are not neglected, our formula takes the form,

$$T = \oint -\frac{\tau^{\ell}}{f_0\rho_0} d\ell + \int_A^C -\left(\frac{RU_s}{f_0}\right) d\ell \quad , \tag{2.14}$$

where U_s is the vertically integrated speed *tangential* to the integration boundary and AC is the part of the ACC that passes through the integration contour (**Fig. 1**). It is difficult to come up with defensible values for the coefficient R but a value of $10^{-6}s^{-1}$ has been used before. It corresponds to a damping time scale of about 11 days which is not unreasonable. Together with relatively high speeds of ~ 0.2 m s^{-1}, a thickness of ~ 500 m and ℓ ~ 1,000 km, we get that the neglected forces can alter our estimate by an amount of O(1 Sv), which is much smaller than our calculated amount (27 Sv).

2.3.4. Potential form-drag effects

Several authors (e.g., Munk and Palmen, 1951; Gille, 1997) have pointed out that the wind stress over the ACC is balanced by topography-induced form-drag. Our contour is, by and large, situated outside the ACC (**Fig. 1**), and we do not expect form-drag to be an issue, but a closer look is warranted. To do so, we note that some models (e.g., Gille, 1997) suggest that the topography-induced drag is confined to a few selected ridges (and this could have been a problem) but satellite data suggest that the drag is more evenly distributed over most of the ACC path. Specifically, Gille (1997) implies that only 15–20% of the total ACC form drag is caused by the Drake Passage. Hence, even if we assume that our contour crosses the ACC's core in the Drake Passage region (which it doesn't), we come up with an estimate that this will not introduce an error larger than 15–20% into our calculation.

3. Numerical simulations

The methodology behind the numerical experiments is the same as that in Nof (2000a, 2002). The main point to recall is that a model whose frictional forces are primarily along WBC will not reach a steady state without sources and sinks as it must obey (2.12) implying that meridional transport must be allowed. The purpose of the numerical simulations is to verify that there are no zonal jets emanating from the tip of the continents and that the zonal flow around Antarctica has no influence on the flow through the contour. Such flows (see, e.g., Nof 2000b) could violate our momentum equations. Also, we wish to verify that these jets and zonal flows are not present regardless of the gap width (the distance between the tip of the continents and Antarctica).

Instead of verifying the above general transport formula (2.13) using very complicated numerical models (corresponding to **Fig. 1**), we examined numerically our first model (**Fig. 3**) which does not contain very complicated geography. Specifically, we considered a layer-and-a-half application of the Bleck and Boudra "reduced gravity" isopycnic model. This numerical model has no thermodynamics, nor does it have enough layers to correctly represent the ACC. Neither of the two is essential at this stage and in order to represent the overturning we introduced sources in the south and sinks in the north. The mass flux associated with these sources and sinks is not *a priori* specified but all sources and sinks are required to handle an identical mount of water (**Fig. 4a**).

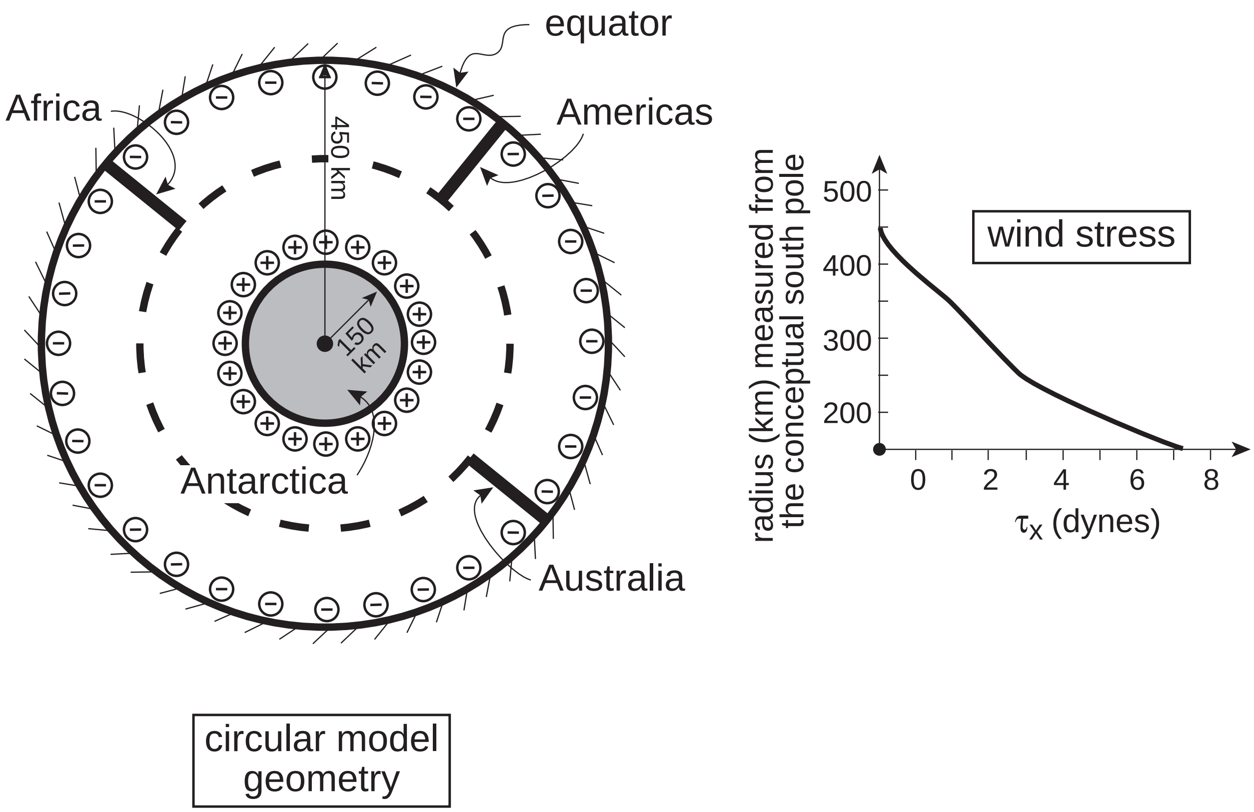

Fig. 4a. Schematics of the (one-and-a-half layer) sources-sinks numerical experiments with the circular basin (Set A). The magnified (and simplified) zonal wind stress as a function of latitude (adapted from Hellerman and Rosenstein, 1983) is shown on the right-hand side. It increases with latitude in concert with the decreasing length of the contour so that the transport T [as given by (2.12)] is a constant. The model has no thermohaline processes in it; instead, the mass flux exiting the (20) sources and entering the (32) sinks represents the meridional flow. It was not specified a priori. Rather, we let the wind blow for a while, measured the transport established across the dashed circle and then required the sinks and sources to accommodate the measured amount. The procedure was then repeated continuously and the sources' mass flux was continuously adjusted until a steady state was reached.

Furthermore, the number of sinks and sources is evenly distributed. This is a matter of choice and consistence with the earlier works (Nof 2000a, 2002) but does not necessarily reflect the actual situation in the ocean as one can easily conceive a scenario where there will be more sinks (and, therefore, more sinking) in one ocean than the other.

As in Nof (2000a, 2002), we let the wind blow, measured the transport established across the contour and then required the sources and sinks to accommodate this measured transport. We continued to do so and continued to adjust the transport until a steady state was ultimately reached. Note that, since our formula gives the transport without giving the complete flow field, it is easiest to start the above runs from a state of rest. Consequently, the initial adjustments that we speak about are not small but they do get smaller and smaller as we approach the predicted transport.

To verify that the computed transport is independent of the gap width (the distance from the edge of Antarctica to the edge of the primarily meridional continents), we first performed a set of experiments where we varied only the gap width in a circular model (**Fig. 4a**) (set A, Table 1). As a second step, we used a rectangular basin with periodic boundary conditions (**Fig. 4b**) and varied the wind stress. We measured the transport, and then plotted the theoretically computed transport versus the numerical transport (set B). To smooth out the fields we began with a relatively large number of sources and sinks (20 sources and 32 sinks in set A). We found that our results were not very sensitive to this choice and, consequently, we reduced the number of sources and sinks dramatically (to 3 sources and 3 sinks) in set B.

3.1. The numerical model

We used a reduced gravity version of the isopycnic model developed by Bleck and Boudra (1981, 1986), and later improved by Bleck and Smith (1990). The advantage of this model is the use of the “Flux Corrected Transport” algorithm (Boris and Book, 1973; Zalesak, 1979) for the solution of the continuity equation. This algorithm employs a higher order correction to the depth calculations and allows the layers to outcrop and stay positive definite. The resulting scheme is virtually non-diffusive and conserves mass. For these reasons, the model is the most suitable model

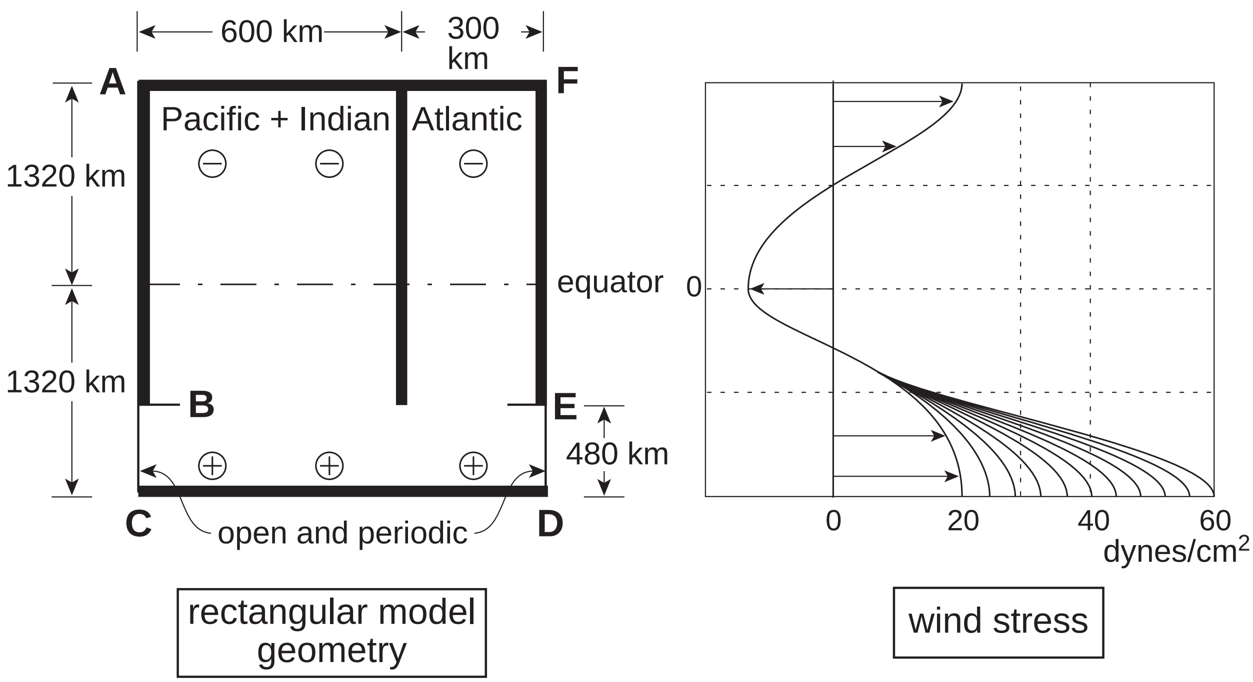

Fig. 4b. The same as **Fig. 4a** except that we show here the rectangular basin (with the periodic boundary conditions) on the left (Set B) and the variable winds on the right. To represent the Southern Ocean, the southern part of the basin was left open on the eastern and western sides. The boundary conditions along ABC and DEF were periodic.

Table 1: A description of the two simulation sets, the variable gap experiments (set A) and the variable wind experiments (set B). The Coriolis parameter f_{max} is measured along the edge of Antarctica (i.e., the solid line in **Fig. 4a** and Section CD in **Fig. 4b**).

<table>
<tr><th>Set</th><th>Exp no.</th><th>Distance between tip of continents and southern boundary (km)</th><th>Δx
Δy
Δt</th><th>R_d</th><th>g'
H
β
ν
K
f_{max}</th><th>mean wind profile magnification factor (approx)</th><th>wind stress along Antarctica dynes/cm^2</th><th>number of sources
———
sinks</th><th>results shown in Fig.</th></tr>
<tr><td rowspan="10">A,
circular
basin
(Fig. 4a)</td><td>1</td><td>150</td><td rowspan="10">15 km
15 km
360 s</td><td rowspan="10">87 km</td><td rowspan="10">0.015 m/s^2
600 m
11.5×10^{-11} m^{-1}s^{-1}
1600 m^{2}s^{-1}
20×10^{-7}s^{-1}
0.345×10^{-4}s^{-1}</td><td rowspan="10">6</td><td rowspan="10">7.3</td><td rowspan="5">20
sources</td><td rowspan="10">5</td></tr>
<tr><td>2</td><td>135</td></tr>
<tr><td>3</td><td>120</td></tr>
<tr><td>4</td><td>105</td></tr>
<tr><td>5</td><td>90</td></tr>
<tr><td>6</td><td>75</td><td rowspan="5">32
sinks</td></tr>
<tr><td>7</td><td>60</td></tr>
<tr><td>8</td><td>45</td></tr>
<tr><td>9</td><td>30</td></tr>
<tr><td>10</td><td>15</td></tr>
<tr><td rowspan="21">B,
rectangular
basin
(Fig. 4b)</td><td>11</td><td rowspan="9"></td><td rowspan="21">15 km
15 km
360 s</td><td rowspan="21">20 km</td><td rowspan="21">0.015 m/s^2
600 m
11.5×10^{-11} m^{-1}s^{-1}
16,000 m^{2}s^{-1}
20×10^{-7}s^{-1}
1.51×10^{-4}s^{-1}</td><td rowspan="21">17</td><td>20</td><td rowspan="10">3
sources</td><td rowspan="21">6, 7, 8</td></tr>
<tr><td>12</td><td>22</td></tr>
<tr><td>13</td><td>24</td></tr>
<tr><td>14</td><td>26</td></tr>
<tr><td>15</td><td>28</td></tr>
<tr><td>16</td><td>30</td></tr>
<tr><td>17</td><td>32</td></tr>
<tr><td>18</td><td>34</td></tr>
<tr><td>19</td><td>36</td></tr>
<tr><td>20</td><td>480</td><td>38</td></tr>
<tr><td>21</td><td rowspan="11"></td><td>40</td><td rowspan="11">3
sinks</td></tr>
<tr><td>22</td><td>42</td></tr>
<tr><td>23</td><td>44</td></tr>
<tr><td>24</td><td>46</td></tr>
<tr><td>25</td><td>48</td></tr>
<tr><td>26</td><td>50</td></tr>
<tr><td>27</td><td>52</td></tr>
<tr><td>28</td><td>54</td></tr>
<tr><td>29</td><td>56</td></tr>
<tr><td>30</td><td>58</td></tr>
<tr><td>31</td><td>60</td></tr>
</table>

for our problem. The modeled basin is either circular (**Fig. 4a**) or a rectangle extending from 70˚S to 70˚N (**Fig. 4b**).

The equations of motion are the two momentum equations,

$$\frac{\partial u}{\partial t} + u\frac{\partial u}{\partial x} + v\frac{\partial u}{\partial y} - (f_0 + \beta y)v = -g'\frac{\partial h}{\partial x} + \frac{\nu}{h}\nabla \bullet (h\nabla u) + \frac{\tau_x}{\rho h} - Ku \tag{3.1}$$

$$\frac{\partial v}{\partial t} + u\frac{\partial v}{\partial x} + v\frac{\partial v}{\partial y} - (f_0 + \beta y)u = -g'\frac{\partial h}{\partial y} + \frac{\nu}{h}\nabla \bullet (h\nabla v) + \frac{\tau_x}{\rho h} - Kv \tag{3.2}$$

and the continuity equation,

$$\frac{\partial h}{\partial t} + \frac{\partial (hu)}{\partial x} + \frac{\partial (hv)}{\partial y} = 0 \tag{3.3}$$

where, as before, the notation is conventional and is given in the Nomenclature.

The model uses the Arakawa (1966) C-grid. The u-velocity points are shifted one-half grid step to the left from the h points, the v-velocity points are shifted one-half grid step down from the h points, and the vorticity points are shifted one-half grid step down from the u-velocity points. This grid allows for reducing the order of the errors in the numerical scheme. The solution is advanced in time using the leap-frog scheme. The velocity fields are smoothed in time in order to stabilize the numerical procedure.

To make our runs more economical, we artificially magnified both β and the wind stress and artificially reduced both the meridional and zonal basin scales (see Table 1 and **Figs. 4a, 4b**). The linear drag coefficient, *K*, was also increased so that the increased wind stress is balanced. With these modifications we had a dramatic reduction in the grid count and, consequently, our runs lasted for about 40 minutes each instead of a week or so that each run would have lasted had we not modified β, the wind stress and the basin's size.

The downside of the above modifications is an unnaturally large ratio between the eddies' size (the Rossby radius) and the basin's size. As we shall shortly see, this is not really a difficulty in our runs because in our case the eddies do not play a major role in the meridional mass exchange. Furthermore, this unnatural eddy-basin-ratio issue can be easily resolved by using a very large horizontal eddy viscosity coefficient that eliminates any long-lived eddies such as Gulf Stream rings. This essentially implies that our model is not an eddy-resolving model. Note also that, even with our large frictional coefficient, the ratio between the Munk layer thickness $(\nu/\beta)^{1/3}$ and the basin size was still very small (as required) because our β is magnified.

3.2. Results

Our results are shown in **Figs. 5, 6, 7 and 8**. **Figs. 5, 6 and 7** show the observed (numerical) transports and their relationship to the analytics. Our eddy viscosity was large in set B (16,000 m^2s^{-1}) so the good agreement between the nonlinear numerical simulations and the quasi-linear analytical computation (no matter how narrow the gap is or how strong the wind is) is not surprising. But the eddy viscosity was not *that large* to kill all the processes that we are interested in and this shows that zonal linear drag and lateral friction (included in the numerics but absent from the analytics) are all unimportant. Furthermore, it shows that, as expected, the large eddy viscosity is compensated by our magnified β and magnified wind stress.

Fig. 5 shows that the results are independent of the gap's width. Even for gaps that are as narrow as 0.2 R_d, our analytical results are in good agreement with the numerics. **Fig. 6** shows that, as the wind stress is increased linearly along the southern coast, both the analytical and the numerical transports increase linearly. However, the analytical transport increases at a rate that is 80% of the numerical growth rate. Since our analytical formula does not involve a detailed solution of the entire flow field, it is very difficult to determine why this is so. One might be tempted to attribute the difference between the two estimates to the linear drag which, though small, is the largest neglected term at least for some of the experiments (see **Fig. 8**). However, since this drag always opposes the throughflow (in the sense that it requires the theoretical transport to be always larger than the numerical), it cannot be the agent responsible for the discrepancy displayed in **Fig. 6**. **Fig. 8** shows the relative importance of the various terms in the integrated momentum equations. We see that, as is assumed in the analytics, lateral friction, linear drag, and advection are all small and negligible.

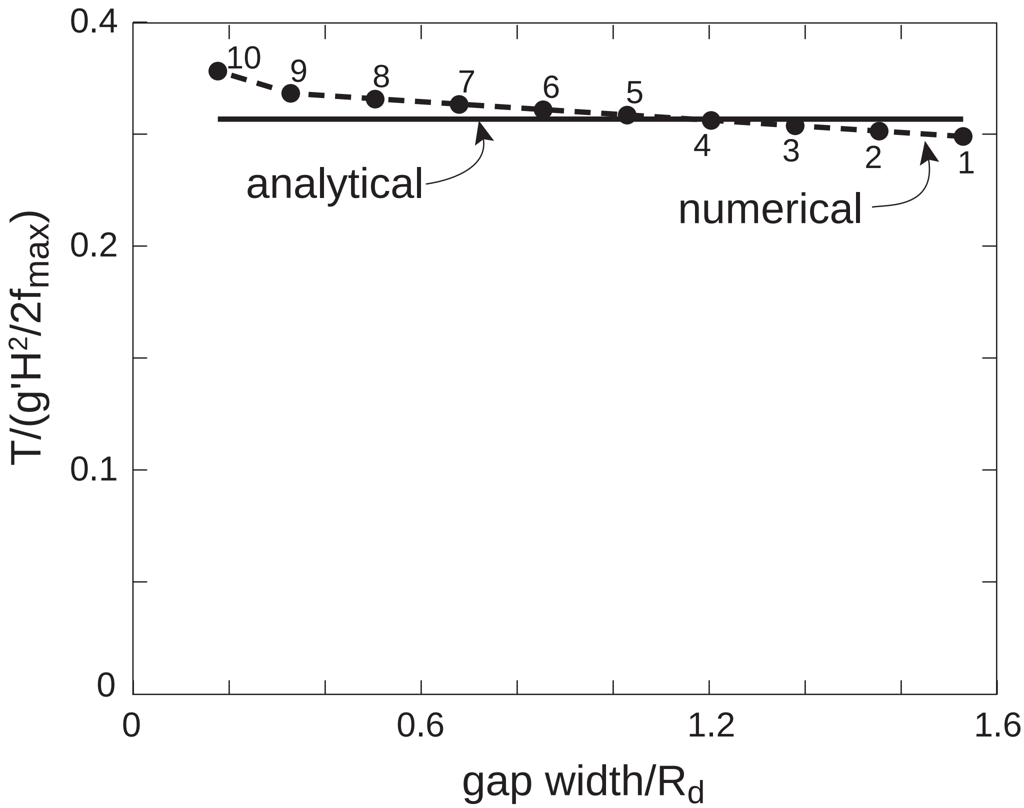

Fig. 5. A comparison between the analytical calculation for the transport (solid line) and the numerical simulations (solid dots) with a variable gap width (Set A). Numerals indicate the experiment number. The transport T is nondimensionalized with $g'H^2/2f_{max}$ where f_{max} is the Coriolis parameter along the southern boundary (Antarctica's border). A comparison between the analytical calculation for the transport (solid line) and the numerical simulations (solid dots) with a variable gap width (Set A). Numerals indicate the experiment number. The transport T is nondimensionalized with $g'H^2/2f_{max}$ where f_{max} is the Coriolis parameter along the southern boundary (Antarctica's border).

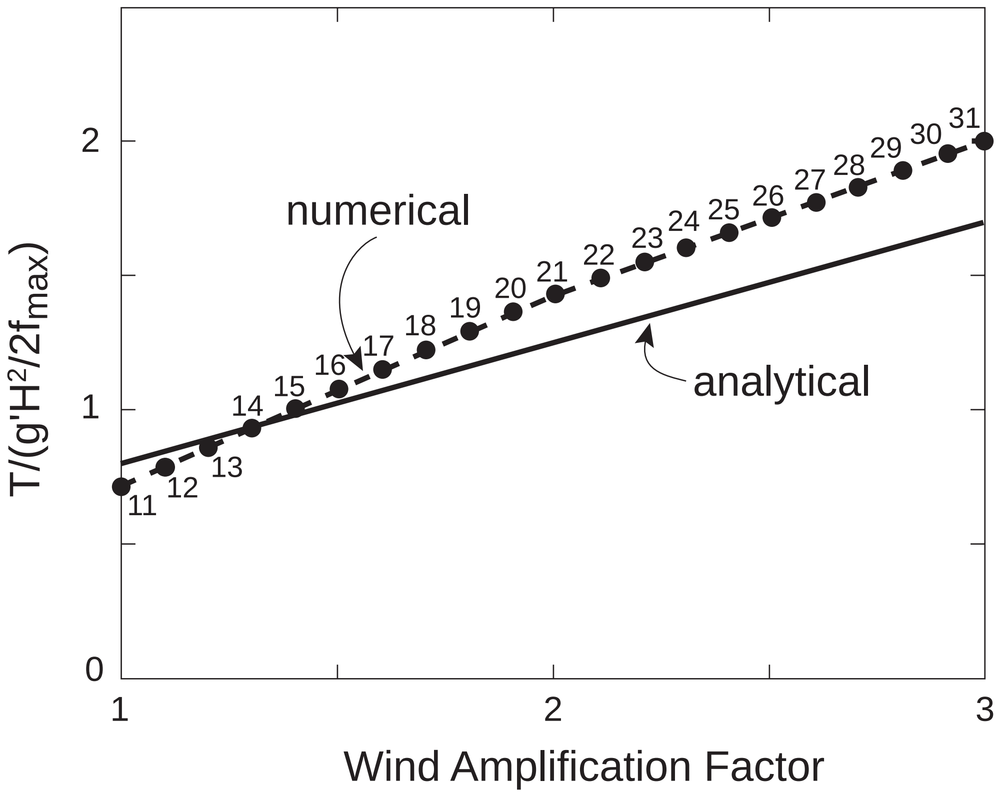

Fig. 6. The same as **Fig. 5** except that we show here the sensitivity of the numerical solution to the variable wind (Set B). The amplification factor is defined as the ratio of the wind along the southern boundary to the wind along the northern boundary (see the right panel in **Fig. 4b**).

Exp 20

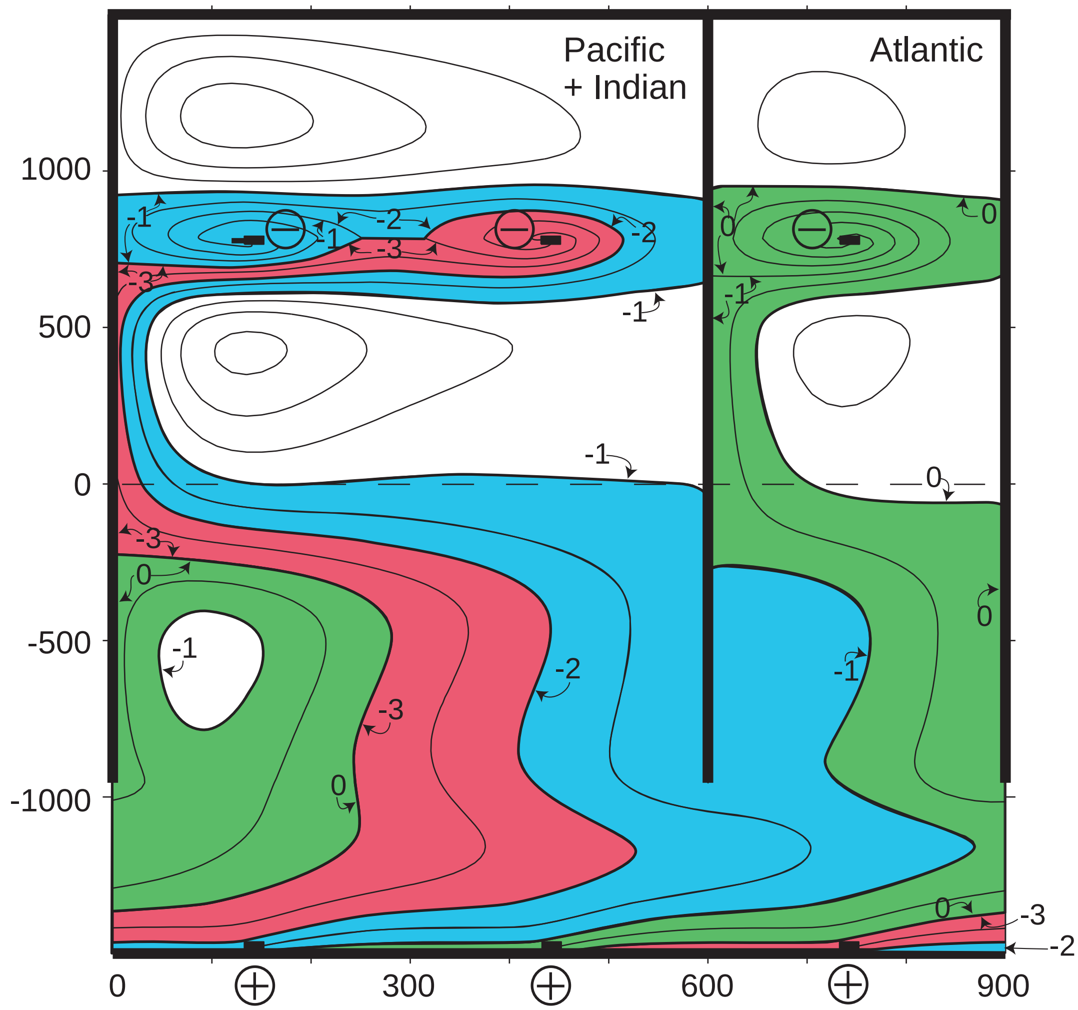

Fig. 7a. The nondimensional transport contours for a typical numerical simulation with a rectangular basin subject to periodic boundary conditions (Set B). The experiment that we show is Exp. 20. Recall that the sinks-sources mass flux is not determined a priori. Rather, the model itself determines the mass flux (see text). Also, recall that the model does not include the dynamics required for the establishment of an ACC. Nevertheless, the model does have a tendency to produce such a current. Note that the Atlantic upper water (green) follows a familiar path. After leaving the Southern Ocean, it loops (in a counterclockwise manner) in the Indian-Pacific Ocean, leaks westward around the western boundary and then follows an "S" shaped path to the North Atlantic where it

ultimately sinks. In addition to this meridional Atlantic circulation, there is a Pacific meridional cell (red and blue) that enters the Pacific from the Southern Ocean, follows an "S" shaped route and sinks (to mid-depth) in the North Pacific.

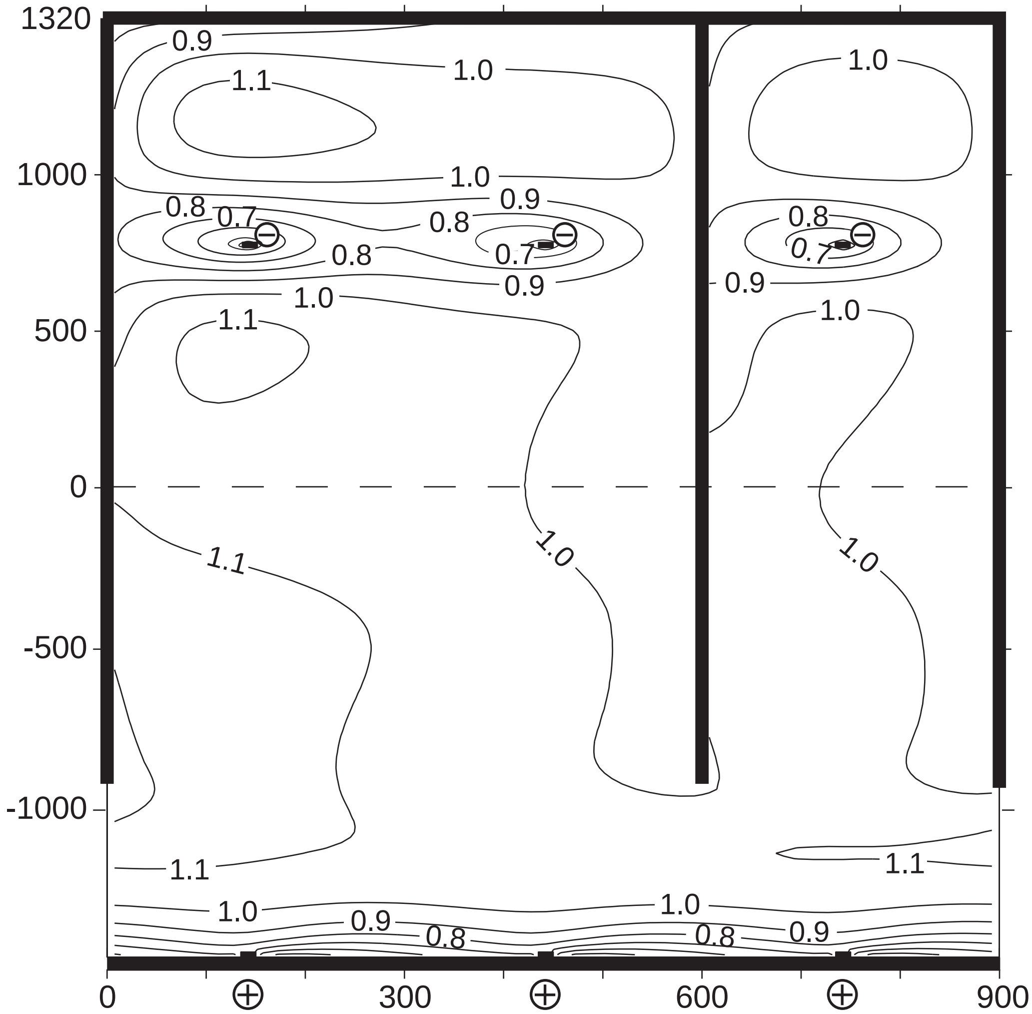

Fig. 7b. Thickness contours for Exp. 20. Non-dimensionalization is done with the undisturbed depth (600 m).

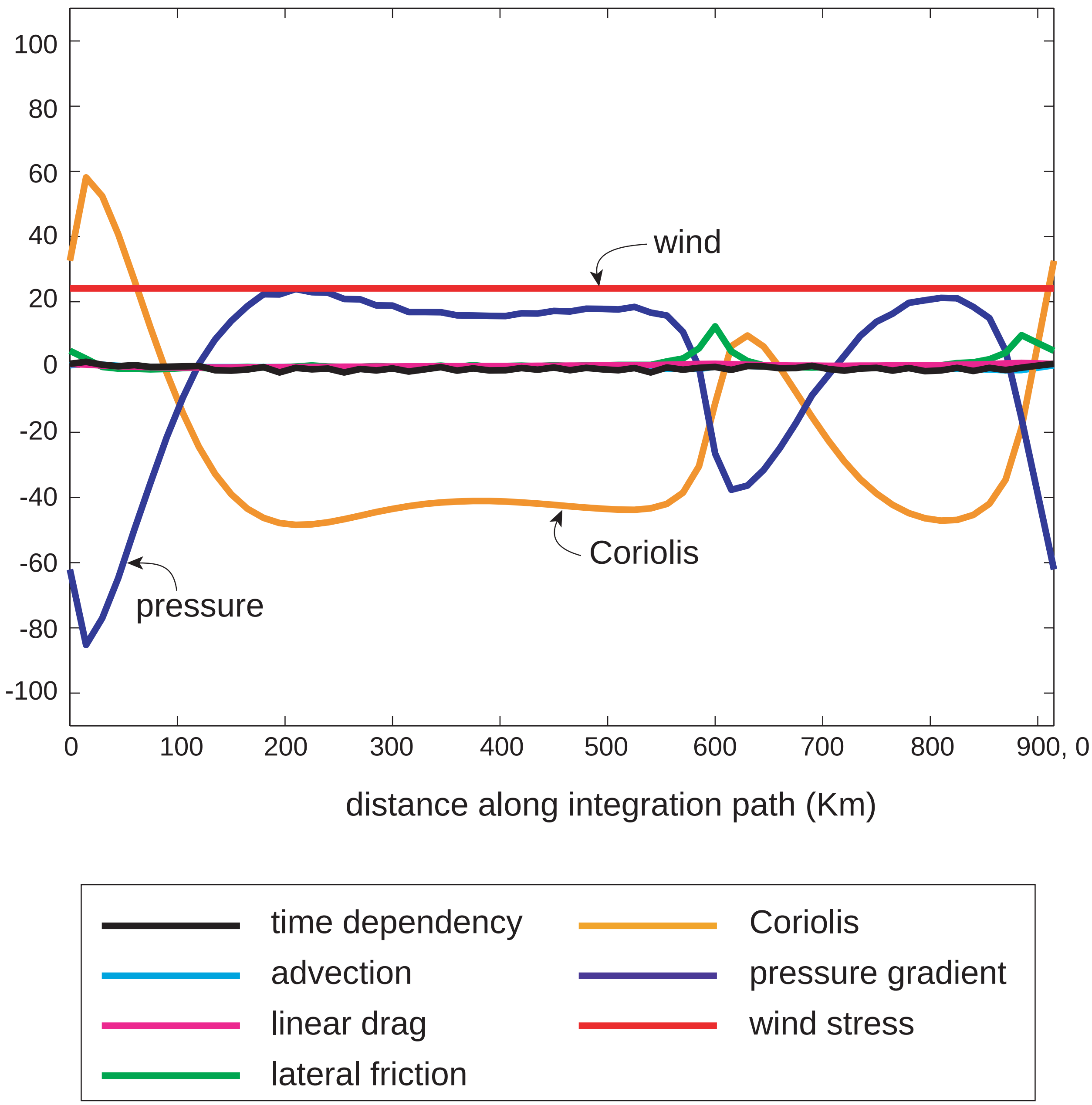

Fig. 8a. A comparison of the various terms in the momentum equation (used to derive the analytical formula) along the closed integration path. Here, we again show Exp. 20 but note that all experiments show very similar results. All the terms which have been assumed to be small in the analytical derivation (time dependency, advection, linear drag, and lateral friction) fall practically on the zero line. The dominant terms are: Coriolis, pressure gradient and wind stress, all of which are included in the analytical derivation.

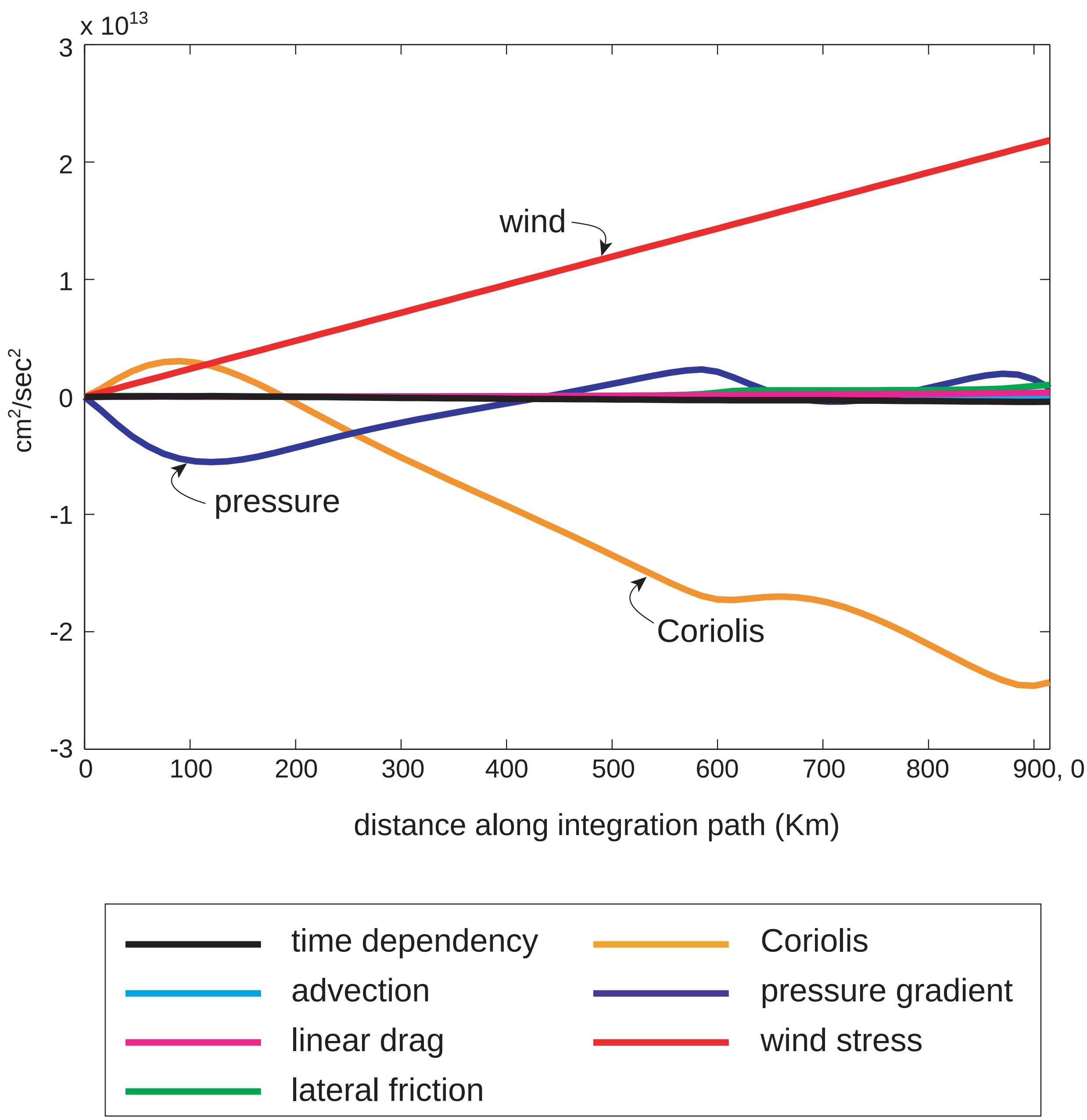

Fig. 8b. The line integrals of the neglected terms shown in **Fig. 8a** and the line integral of the wind stress. Note that the neglected integrated advection, lateral friction, linear drag and time dependency are also almost zero as should be the case.

Fig. 7 also shows how the two MOCs cross the equator. The water that ultimately sinks in the North Atlantic (green) first loops in the Indian-Pacific Ocean in the familiar counterclockwise manner. This loop is caused by the ACC which pushes this MOC eastward. The water then enters the southeastern Atlantic through the (linear) interior. Finally, it follows an "S" shaped path and reaches the North Atlantic. One of the most important aspects of **Fig. 7a** is that it shows very vividly that the waters entering the northern oceans are not Ekman fluxes but Sverdrup interior waters (along the eastern boundaries). For instance, in the Atlantic, it is the green water (but not the blue) that ends up in the northern hemisphere and in the Pacific-Indian system it is the red and the blue (but not the green) that ends up in the opposite hemisphere. This point will be further discussed in section 5.

It should be stressed that, although the agreement between the analytics and the numerics is informative, the numerical simulations do not completely validate our analytical results as, in order to do so, it is necessary to use a model with thermodynamics. Specifically, it is necessary to conduct experiments with variable diabatic forcing and constant wind and show that the northward transport remains constant. These aspects are presently examined and will be reported elsewhere.

4. The new calculated meridional transport

We used NCEP Reanalysis data[1] for annual mean winds (averaged over 40 years) with a drag coefficient of 1.6×10^{-3} [which is the appropriate coefficient for winds (such as ours) with a speed of less than 6.7 m s^{-1} (see e.g., Hellerman and Rosenstein (1983)]. Along the chosen path (**Fig. 1**), the integration was done over $2^{\circ} \times 2^{\circ}$ boxes. With the aid of (2.13) one finds a reasonable net meridional transport of about 29 Sv. According to the NCEP data for our contour, the winds do not vary much with longitude suggesting that the relative spacing between the continents can be used to divide the 29 Sv between the Atlantic (9 Sv) and the Pacific-Indian system (20 Sv). Also, the corridor that (2.13) applies to is so narrow that the variation of the wind across it is not important.

Before proceeding and discussing the implication of this calculation, it is appropriate to discuss two limitations of our analysis.

i. *Agulhas rings*. Both observations and wind-driven circulation models show that there is a transfer of Indian Ocean thermocline water into the South Atlantic (Boudra and Chassignet, 1988; Semtner and Chervin, 1988; Gordon and Haxby, 1990). Most of the leakage is achieved via Agulhas rings (Olson and Evans, 1986; Lutjeharms and Gordon, 1987; Lutjeharms and Van Ballegooyen, 1988), but additional Indian Ocean waters are injected into the Atlantic via plumes (Olson and Evans, 1986; Lutjeharms, 1988; Lutjeharms and Valentine, 1988). Also, surface water are sometimes entrained by the Benguela Current (Nelson and Hutchings, 1983; Shannon, 1985). Estimates of the above leakages vary considerably due to various measuring techniques and (perhaps) due to actual variability.

[1] Provided by the NOAA-CIRES Climate Diagnostics Center, Boulder, Colorado, from their Web site at http://www.cdc.noaa.gov.

Gordon et al. (1987) arrived at an estimate of 10 Sv for water entering the Atlantic in 1983 whereas Whitworth and Nowlin (1987) observed a much larger transport of 20 Sv in 1984. Bennett (1988), on the other hand, arrived at lower values of 6.3 and 9.6 Sv for 1983 and 1984. From these amounts that enter the Atlantic, Bennett argued that only 2.8 Sv are warm Indian Ocean water. Stramma and Peterson (1990) found an Indian to Atlantic transfer of 8 Sv whereas Gordon and Haxby's (1990) inventory of rings suggested a transport of 10–15 Sv. McCartney and Woodgate-Jones' (1991) definition of an eddy corresponded to a smaller feature than that considered by Gordon and Haxby (1990) and, consequently, they arrived at a smaller estimate of 2–5 Sv. Byrne et al. (1995) estimated the flux to be at least 5 Sv; the most recent and most extensive estimate is that of Goñi et al. (1997), who arrived at an average influx of no more than 4–5 Sv. Since it is the most updated estimate we shall use this latter value as a typical mass flux of warm Indian Ocean water into the South Atlantic [even though it is somewhat smaller than previous values (see also Van Ballegooyen et al., 1994 and Duncombe Rae et al., 1996)].

Olson and Evans (1986) estimate that the rings translate toward the northwest at a rate of 5–8 cm sec^{-1} whereas Goñi et al. (1997) arrive at a rate of 5–14 cm sec^{-1}. A fourth of this speed is probably due to the familiar β-induced speed which, for rings with a diameter of 400–500 km, a depth of 800 m, and a reduced gravity of 2×10^{-2}m s^{-2}, is no more than 1.5 cm s^{-1}. [This can be easily verified by recalling that such rings translate at a speed that is smaller than $0.4\ \beta R_d^2$ where R_d is the Rossby radius based on the ring's maximum depth (see e.g., Nof, 1981).] Another fourth of the observed migration speed is due to advection by the local Sverdrup flow (see **Fig. 6**) and the remaining half (3–7 cm sec^{-1}) cannot be clearly accounted for. [It can possibly be due to bottom topography which increases the migration rate (see e.g., Dewar and Gailliard, 1994 but also Kamenkovich et al., 1996 where a counter-example of a reduced rate is given) or due to a dipolar structure (Radko, 1997).] Regardless of the cause for this unaccounted speed, we can conclude that out of the 4–5 Sv influx, about 1.5 Sv is due to advection by the surrounding flow that obeys Sverdrup dynamics and, hence, is *included* in our calculations. Namely, in our calculations, 3–4 Sv are neglected because of the absence of the rings' self-propulsion mechanism. Although definitely not entirely negligible, this is a relatively small amount compared to the observed 10 Sv or so of the inter-hemispheric flow that enters the South Atlantic. Before concluding this subsection it should be pointed out that there is no general agreement on what the transport of Agulhas rings is and some may prefer to stick with the original estimates of Gordon (1986) giving 10 Sv or so.

ii. <u>*Eastern boundary currents*</u>. Eastern boundary currents in the southeastern Atlantic and the southeastern Pacific (neglected in both the analytics and numerics) may also affect the calculation. Recent measurements of the Benguela Current (Peterson and Stramma 1991; Clement and Gordon 1995; Garzoli et al. 1996; Garzoli et al. 1997) suggest, however, that there is a difference of merely a few Sverdrups between the calculated Sverdrup transport (included in both the analytical and the numerical models) and the measured Benguela Current transport. There are no direct measurements of the southeast corner of the Pacific but overall, we can say that all eastern nonlinear processes (e.g., Agulhas ring, the Benguela Current, the Norwegian Current) may affect our estimation by a few or several Sverdrups.

Before proceeding, we should perhaps stress once more that the integration path is, by and large, *outside* the ACC. The only section where the integration path crosses the ACC (and the momentum balance used to derive our transport formula could be violated) is the Drake Passage and its immediate vicinity (AC in **Fig. 1**). Since this section is small compared to the entire integration path and, since the actual form drag exerted by the Drake Passage on the ACC is no more that 15–20% of the entire ACC bottom drag (see e.g., Gille, 1997), the error introduced by this crossing (of the ACC) is small. Finally, note that, as mentioned, there is very little room between the southern tips of the continents and the northern edge of the ACC to fit the integration contour. This implies that the sensitivity of the computed transport to the particular choice of the integration path (and its associated wind dependency) is minimal.

5. Does (2.12) coincide with the actual Ekman transport across the contour?

At first glance, (2.12) and (2.13) give the erroneous impression that the northward Ekman transport across the contour actually represents the MOC, i.e., that the fluid that starts in the Southern ocean and ends up in the northern hemisphere coincides with the Ekman transport across the contour shown in **Fig. 1**. A careful examination shows that this is not the case as the fluid that constitutes the MOC corresponds to either a fraction of the northward Sverdrup transport or a fraction of the WBC (rather than the Ekman transport). It is merely that the amount of water that is flowing northward is identical to the amount of the Ekman transport. To see this we first note that nowhere in our solution and its derivation has it ever been mathematically stated whether the flow belongs to the WBC, the Sverdrup interior or the Ekman flow. The only statement that has been made is that it is a combination of the three because (2.12) corresponds to an integrated quantity. We shall see that how the flow is partitioned between the Sverdrup and the WBC is determined by the *wind stress curl* which is not even present in (2.12).

We shall use two examples to show this. First, we shall look at the general case where there is a Sverdrup transport in the interior (**Fig. 9**) and then we shall look at the special case where $\partial\tau/\partial y \; \underset{\cdot}{\tilde{\equiv}}$ everywhere in the basin (**Fig. 10**). The second case is highly simplified and is, therefore, easier to understand. Some readers may prefer to look at it first.

<u>Example 1:</u> Consider the southern boundary of the Atlantic and assume, for simplicity, that $\partial P^*/\partial x$ integrates to zero not only over the entire contour around the globe but also in each of the individual oceans. Suppose, for a moment, that there is no MOC [i.e., the integral of (2.12) gives zero] so that the WBC transport (say, 40 Sv) is equal to and opposite that of the Sverdrup transport to the east (40 Sv). In this case $\tau = 0$ along our integration contour but $\partial\tau/\partial y$ is not zero. This is shown in the upper panel of **Fig. 9**. Next, consider the case where $\partial\tau/\partial y$ remains the same as before but τ is no longer zero along AB. Suppose further that (2.12) gives 10 Sv for AB. Since the Sverdrup transport is fixed by the wind, the only way for the ocean to accommodate this northward transport of 10 Sv (imposed by the nonzero wind stress) is to weaken the WBC (from 40 to 30 Sv). The weakened WBC (**Fig. 9**, lower panel) still forms a recirculating gyre of 30 Sv with the western part of the Sverdrup transport (unshaded region) and, consequently, its fluid never leaves the southern hemisphere. The remaining Sverdrup transport (10 Sv) which does not participate in this recirculating gyre corresponds to the MOC, i.e., the fluid that ultimately

crosses the equator and ends up in the northern hemisphere (shaded region). This is the fluid that we are interested in. It is situated next to the eastern boundary and corresponds to 1/4 of the total Sverdrup transport. This MOC transport is of the same amount as that given by the Ekman transport across AB but it

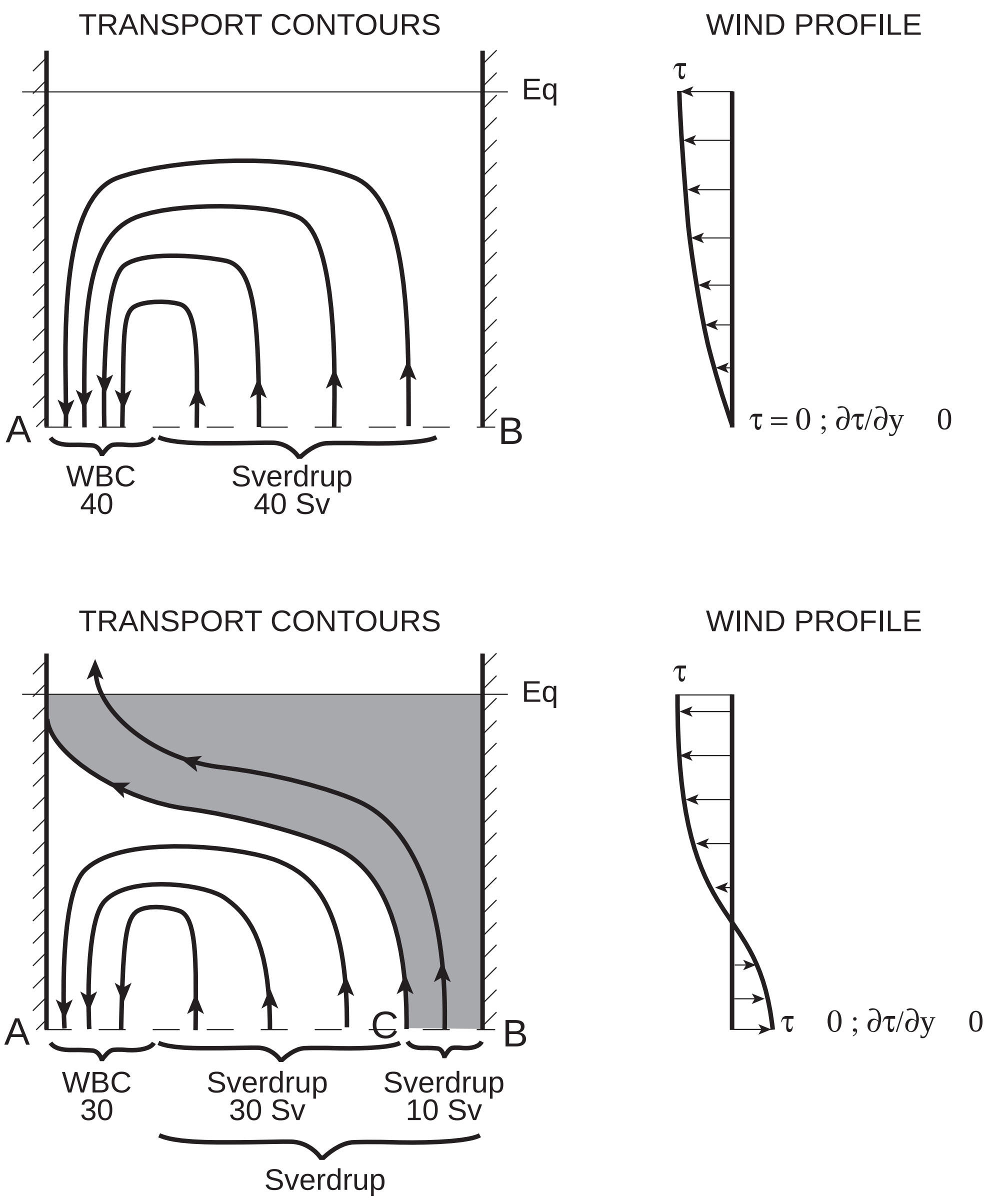

Fig. 9. A cartoon of the South Atlantic flow pattern in the vicinity of the integration contour. In the upper panel we show the case where (2.12) gives zero, i.e., there is no MOC and the WBC transport (say, 40 Sv) is equal and opposite to the Sverdrup flow. In the lower panel we show the case where the curl of the wind stress is the same as above but the

integral of the wind stress across AB is now nonzero (and gives 10 Sv), i.e., there is an MOC. Since the Sverdrup balance is fixed by the wind, the only way for the ocean to accommodate the MOC is to weaken the WBC (from 40 to 30 Sv). As a result, the Sverdrup transport (still 40) is now greater than the WBC (30 Sv) and 10 Sv are now flowing northward along the eastern boundary. This 10 Sv ultimately ends up in the northern hemisphere (shaded). The northward flowing 10 Sv is also the calculated Ekman transport across AB but corresponds to a different water mass. Most of the Ekman flux across AB (i.e., the Ekman transport associated with AC) is advected by the fluid below in a circulatory manner and never crosses the equator because it is flushed out of the South Atlantic.

obviously corresponds to a different water mass. Most of the Ekman transport across AB (the part between A and C) is advected by the fluid below in a manner that does not allow it to cross the equator, i.e., whatever enters this (unshaded) region is flushed back to the Southern Ocean.

How is this reconciled with the fact that the integral of the geostrophic flow underneath the Ekman layer is zero? Very simply, the fact that there is no net flow in the geostrophic interior does not at all mean that the water that gets into the basin through AB is the *same* water that gets out via the WBC. All that it means is that there will be *some* water of the same amount that leaves through the interior. So, the amount of water going northward through AB (shaded region in the lower panel of **Fig. 9**) is *equal* to the Ekman transport across AB but constitutes a different water mass than the actual Ekman transport. As we have seen above, most of the entering Ekman transport is flushed back out of the South Atlantic (through the the fluid below).

It should be kept in mind, of course, that the above analysis is based on the vertically integrated equations. A detailed picture of the actual particles path (Ekman and interior) can only be provided by very detailed modeling which is beyond the scope of this study.

<u>Example 2:</u> Consider now the special (hypothetical) case of $\partial\tau/\partial y \equiv 0$ everywhere (no Sverdrup transport). Here, the MOC is flowing northward as a WBC with a transport

equal to that of the Ekman transport across AB (**Fig. 10**). To see this, note that, since there is no Sverdrup transport east of the WBC, the northward Ekman transport there (10 Sv, shown in green) is compensated for by a southward transport of 10 Sv immediately underneath (yellow). Namely, the interior Ekman transport (green) proceeds meridionally all the way to the equator which acts like a wall (for the interior). Immediately south of the equator the Ekman transport sinks and returns southward as an interior geostrophic flow (yellow).

Since the geostrophic interior transport must integrate across to zero, the southward transport underneath the Ekman layer (yellow) is compensated for by a northward WBC of 10 Sv (light blue). This WBC represents the MOC which ends up in the northern

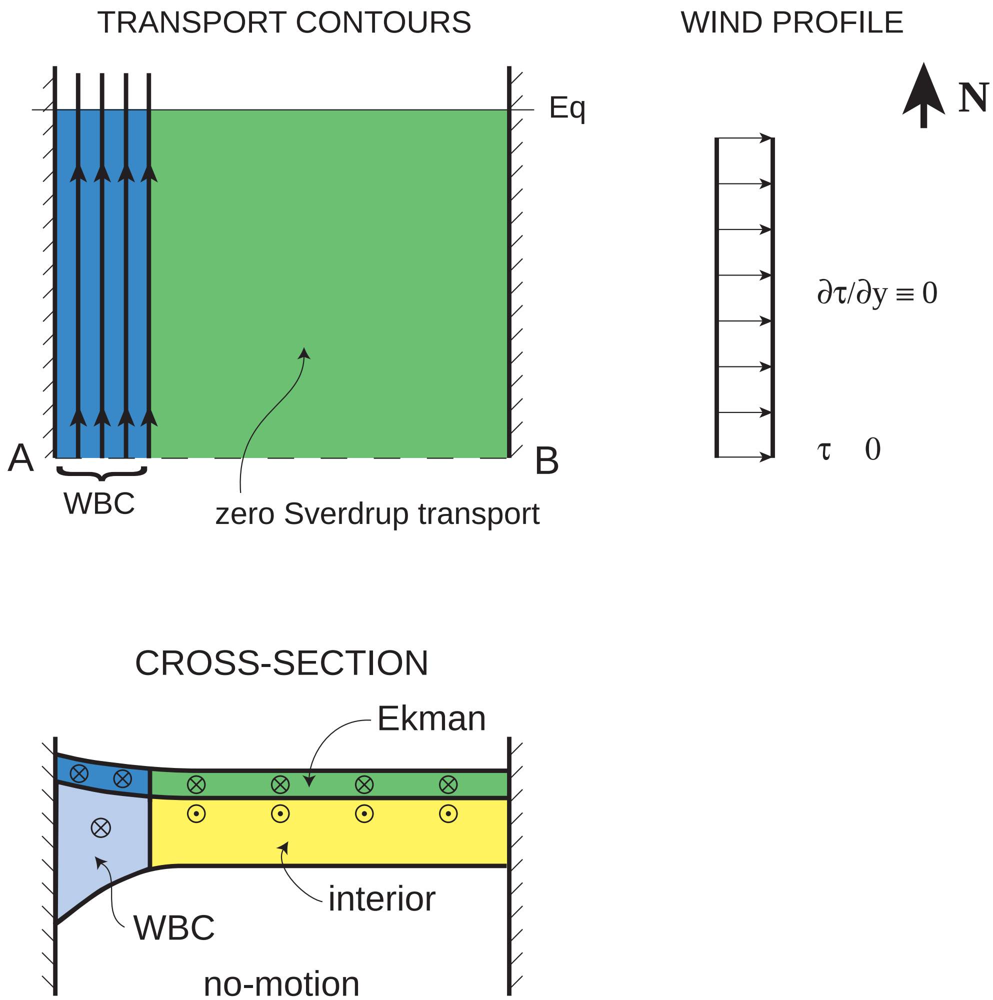

Fig. 10. The hypothetical (special) case of an MOC with no Sverdrup transport (i.e., $t \neq 0$ but $\partial t/\partial y \int 0$ everywhere). Here again, most of the Ekman transport across AB (green) does not participate in the MOC drama even though the WBC transport (2.12) is the same as the Ekman transport. Since there is no net meridional transport east of the WBC, the northward Ekman transport there (10 Sv shown in green) cannot cross the equator, and hence, it sinks immediately to the south of it. This Ekman transport (green) is compensated for by a southward geostrophic flow immediately underneath (yellow). In turn, this interior flow underneath the Ekman layer (yellow) creates a compensating northward flowing WBC (light blue) which also carries 10 Sv. Namely, since the geostrophic interior flow must integrate to zero, the northward WBC is established to compensate for the southward geostrophic flow underneath the Ekman layer (yellow). Note that the amount of water associated with the Ekman flux within the WBC region

(dark blue) is very small compared to the total Ekman flux (green plus dark blue) because the WBC is much narrower than the basin.

hemisphere. Again, although its transport is equal to that of the Ekman transport, it constitutes an entirely different water mass (i.e., blue rather than green). Note that the Ekman transport within the WBC (dark blue) is negligible compared to the total Ekman flux because the scale of the WBC is much smaller than the basin scale.

This completes the description of our two examples. A final point to be made is that the only time when (2.12) does coincide with the Ekman transport is when,

$$\int_A^B \frac{1}{\beta}\frac{\partial \tau}{\partial y}\,dx = \int_A^B \frac{\tau}{f_0}\,dx \quad ,$$

where A and B are shown in **Fig. 9**. In this case the Ekman transport is identical to the Sverdrup transport because there is no WBC! Of course, this is not a realistic case as the actual WBC across the contour in question is almost 100 Sv (the sum of the Agulhas and the Brazil Current transports).

6. Summary and discussion

We have addressed three different calculations of the meridional transfer of upper and intermediate water from the Southern Ocean to low latitude oceans. The first two are recent quasi-island calculations (Nof 2000a, 2002) where the continents are taken to be islands in the sense that they are entirely surrounded by water but there is no significant circulation around them (i.e., there is very little flow through the Bering Strait). These calculations show that 9 Sv enter the Atlantic (forming a top-to-bottom MOC) and 18 Sv enter the Pacific-Indian system (forming a top-to-mid-depth MOC). One of the main weakness of these recent calculations is the neglect of the form drag associated with the Bering Strait sill. This neglect may introduce an error of several Sverdrups to the calculation. The sign of the error is not, however, undetermined. Observations suggest that the isopycnals shoal as one proceeds from the Pacific to the Arctic (through the Bering Strait), indicating that the above error can only subtract from the 18 Sv estimate for the shallow MOC in the Pacific and add to the 9 Sv estimate for the MOC in the Atlantic.

We have presented here complementary new calculations where the linearized equations of motion are integrated around a latitudinal belt. In these new calculations there is no Bering Strait so that the above main weakness of the earlier studies is removed. In this new context, we have considered two new analytical models. The first is a circular model subject to both thermohaline processes and zonal winds (**Fig. 3**). The vertical structure corresponds to four layers of which only the top is explicitly represented in the model (**Fig. 3b**). This top layer includes the Ekman transport, the geostrophic transport underneath and the WBC transport. Underneath this shallow top layer there is a thick intermediate layer whose motions (but not necessarily the transports) are small and negligible. Under these two layers there are two deep layers which require the presence of deep meridional walls in order to exist. The first of these carries water such as the NADW southward whereas the second carries the AABW northward. It is assumed here that the vertical extent of these walls and sills is below our level of no-motion.

The second new model is a more "realistic" model in the sense that it is subject to both zonal and meridional winds (**Fig. 1**) and to more complicated geometry. In both of these new models the interior is governed by Sverdup dynamics and the WBC is dissipative in nature. Surface cooling and heating are allowed everywhere and need not be specified. Some nonlinearity is included (through the pressure terms) but the inertial terms are neglected and the motions are primarily geostrophic.

Our analytical solution for both new models enables one to obtain the net northward transports (of thermocline and intermediate water) directly from the wind field and the geography. The derivation of the analytical solution is based on the fact that the integral of the (upper layer) pressure gradient $\partial P^*/\partial \ell$ along a closed contour (ℓ) vanishes. (Note, however, that the integral of the pressure gradient in the deep layers, which require meridional walls and are not included in the model, would not, in general, vanish.) The new analytical results were compared in detail to new numerical simulations using two isopycnic models (without thermodynamics) and a good agreement was found (**Figs. 5, 6, 7 and 8**). One of these two new models is circular and the other is rectangular with periodic boundary conditions (**Figs. 4a, 4b**). The comparison shows that the results are not very sensitive to the problem parameters (i.e., the width of the gap or the strength of the winds) and that the neglected terms are indeed small. It is worth pointing out here that, since the theoretical problem is linear, the solutions are additives so that any solution can be super-imposed on a known solution.

The calculation of the transport associated with the second new analytical (realistic) model was obtained by using 40 years of NCEP data. The transport derived in this fashion contains some of the Agulhas rings' mass flux save the self-propelled transport. Note that, given the relatively short spacing between the northern edge of the ACC and the southern tips of the continents (**Fig. 1**), as well as the size of our averaging boxes ($2^\circ \times 2^\circ$), it is practically impossible to choose a much different integration. We found that the total calculated northward transport is about 29 Sv which, in view of the spacing between the tips of the continents and the lack of significant wind variability with longitude, gives that 9 Sv enter the Atlantic and 20 Sv enter the Pacific-Indian system. [For a comparison, it is perhaps appropriate to point out that the actual Ekman transport across the contour shown in **Fig. 1** (i.e., the transport calculated on the basis of the local Coriolis parameter) is 27 Sv, which is very close to our approximated flux of 29 Sv.] It is estimated that the Benguela Current, Agulhas rings, and other nonlinear processes may add or subtract several Sverdrups to the above transport. AABW entering the lower latitude oceans from the Southern Ocean (several Sverdrups) is not included in the above estimate.

The new results are in surprisingly good agreement with the earlier quasi-island calculations. Our present new calculation of 9 Sv flowing into the Atlantic from the Southern Ocean is in agreement with the 9 Sv found by the pseudo-island calculation of Nof (2000a), and our present calculation of 20 Sv entering the Indian-Pacific system is also in excellent agreement with the 18 Sv calculated by Nof (2002) using the pseudo-island model. With our simplified models one would normally expect a much larger discrepancy and the excellent agreement is probably fortuitous.

In summary, it is suggested that the transport of upper and intermediate water into the Pacific-Indian and Atlantic can be estimated from the wind field over the Southern Ocean. It is pointed out that this transport does not coincide with the local Ekman transport across the contour (**Figs 9 and 10**). The main error in our calculation is due to the linearization of the ocean's interior which involves the neglect of the nonlinear self-propulsion of Agulhas rings, meridional eddy fluxes, and the friction of eastern boundary currents. All of these processes can probably affect our results by several Sverdrups.

Finally, the reader may find it peculiar that, as in the quasi-island calculations, we were able to compute the overturning limb without explicitly specifying the transformation of light to heavy water. As pointed out in the text, this is due to the fact that the density transformation does not control the net northward flux along the latitudinal belt connecting the southern tip of the continents. This flux is entirely controlled by the wind; the density transformation merely controls the local sinking and upwelling occurring within the limits of the oceans to the north of the Southern Ocean.

7. Acknowledgements

This study was supported by the National Science Foundation contract OCE 9911324; National Aeronautics and Space Administration grants NAG5-7630, NGT5-30164, and NAG5-10860; Office of Naval Research grant N00014-01-0291; and Binational Science Foundation grant 96-105. Discussions with G. Weatherly were very useful. Computations were done by S. Van Gorder and drawings by Beth Raynor.

7. Nomenclature

T	total transport
f	Coriolis parameter
f_ℓ	average Coriolis parameter along the integration belt
f_0	average Coriolis parameter along the contour
f_{max}	maximum Coriolis parameter
ℓ	component along the integration
k	vertical eddy diffusivity
K	linear drag coefficient
P	deviation of the hydrostatic pressure from the pressure associated with a state of rest
R	interfacial friction coefficient
T	temperature
u,v,w	velocities in the x, y and z directions
U,V	vertically integrated transports in the x and y directions
w	vertical velocity
η	free surface vertical displacement
ρ'	density deviation
ρ_0	reference density
τ	wind stress
τ^ℓ	wind stress component along the integration path
ξ	depth of the level of no horizontal pressure gradient

8. References

Arakawa, A., 1966. Computational design for long-term numerical integration of the equations of fluid motion. Two dimensional incompressible flow. Part I, *J. Comput. Phys.,* **1**, 119-143.

Bennett, S. L., 1988: Where three oceans meet: The Agulhas retroflection region. Unpublished Ph.D. Thesis, MIT/WHOI, WHOI-88-51, xxvii + 367 pp.

Bleck, R. and D. Boudra, 1981: Initial testing of a numerical ocean circulation model using a hybrid, quasi-isopycnic vertical coordinate. *J. Phys. Oceanogr.,* **11**, 744-770.

Bleck, R. and D. Boudra, 1986: Wind-driven spin-up in eddy-resolving ocean models formulated in isopycnic and isobaric coordinates. *J. Geophys. Res.,* **91**, 7611-7621.

Bleck, R. and L. T. Smith, 1990: A wind-driven isopycnic coordinate model of the North and Equatorial Atlantic Ocean, 1, Model development and supporting experiments. *J. Geophys. Res.,* **95**, 3273-3285.

Boris, J. P. and D. L. Book, 1973: Flux-corrected transport. I. SHASTA, a fluid transport algorithm that works. *J. Comput. Phys.,* **11**, 38-69.

Boudra, D. B. and E. P. Chassignet, 1988: Dynamics of Agulhas retroflection and ring formation in a numerical model. Part I: The vorticity balance. *J. Phys. Oceanogr.,* **18**, 280-303.

Byrne, D. A., A. L. Gordon and W. F. Haxby, 1995. Agulhas eddies: A synoptic view using Geosat ERM data. *J. Phys. Oceanogr.*, **25**, 902-917.

Clarke, A. J., 1982: The dynamics of large-scale, wind-driven variations in the Antarctic Circumpolar Current. *J. Phys. Oceanogr.*, **12**, 1092-1105.

Clement, A. C. and A. L. Gordon, 1995: The absolute velocity field of Agulhas eddies and the Benguela Current. *J. Geophys. Res.*, **100**, 22591-22601.

Dewar, W. K. and C. Gailliard, 1994: The dynamics of barotropically dominated rings. *J. Phys. Oceanogr.*, **25**, 5-29.

Döös, K., 1994: Semianalytical simulation of the meridional cells in the Southern Ocean. *J. Phys. Oceanogr.*, **24**, 1281-1293.

Duncombe Rae, C. M., S. L. Garzoli, and A. L. Gordon, 1996: The eddy field of the southeast Atlantic Ocean: A statistical census from the BEST project. *J. Geophys. Res.*, **101**, 11949-11964.

Garzoli, S.L., A. L. Gordon, V. Kamenkovich, D. Pillsbury and C. Duncombe-Rae, 1996: Variability and sources of the southeastern Atlantic circulation. *J. Mar. Res.*, **54**, 1039-1071.

Garzoli, S. L., G. J. Goñi, A. J. Mariano, and D. B. Olson, 1997: Monitoring the upper Southeastern Atlantic transports using altimeter data. *J. Mar. Res.*, **55**, 453-481.

Gill, A. E. and E. H. Schumann, 1979: Topographically induced changes in the structure of an inertial coastal jet: Application to the Agulhas Current. *J. Phys. Oceanogr.*, **9**, 975-991.

Gill, A. E. and K. Bryan, 1971: Effects of geometry on the circulation of a three-dimensional southern-hemisphere ocean model. *Deep-Sea Res.*, **18**, 685-721.

Gille, S. T., 1997: The Southern Ocean momentum balance: Evidence for topographic effects from numerical model output and altimeter data. *J. Phys. Oceanogr.*, **27**, 2219-2232.

Godfrey, J. S., 1989: A Sverdrup model of the depth-integrated flow for the world ocean allowing for island circulations. *Geophys. Astrophys. Fluid Dynamics,* **45**, 89-112.

Goñi, G. J., S. L. Garzoli, A. J. Roubicek, D. B. Olson and O. B. Brown, 1997: Agulhas ring dynamics from TOPEX/POSEIDON satellite altimeter data. *J. Marine Res.,* **55**, 861-883.

Gordon, A. L. and W. F. Haxby, 1990: Agulhas eddies invade the South Atlantic: Evidence from geosat altimeter and shipboard conductivity-temperature-depth survey. *J. Geophys. Res.,* **95**, 3117-3127.

Gordon, A. L., 1986. Inter-ocean exchange of thermocline water. *J. Geophys. Res.,* **91**, 5037-5050.

Gordon, A. L., J. R. E Lutjeharms and M. L. Gründlingh, 1987: Stratification and circulation at the Agulhas retroflection. *Deep-Sea Res.*, **34**, 565-599.

Hellerman, S. and M. Rosenstein, 1983: Normal monthly wind stress over the world ocean with error estimates. *J. Phys. Oceanogr.,* **13**, 1093-1104.

Ivchenko, V.O., K. J. Richards and D. P. Stevens, 1996: The dynamics of the Antarctic Circumpolar Current. *J. Phys. Oceanogr.*, **26**, 753-774.

Johnson, G. C. and H. L. Bryden, 1989: On the size of the Antarctic Circumpolar Current. *Deep-Sea Res.*, **36**, 39-53.

Kamenkovich, V. M., 1962: K teorii Antarktichekogo Krugovogo Techeniya (On the theory of the Antarctic Circumpolar Current). *Trud. Inst. Okeanologii AN SSSR*, **56**, 241-293.

Kamenkovich, V. M., Y. P. Leonov, D. A. Nechaev, D. A. Byrne, and A. L. Gordon, 1996: On the influence of bottom topography on the Agulhas eddy. *J. Phys. Oceanogr.*, **26**, 892-912.

Killworth, P.D., 1991: Cross-equatorial geostrophic adjustment. *J. Phys. Oceanogr.,* **21**, 1581-1601.

Killworth, P. D. and M. M. Nanneh, 1994: On the isopycnal momentum budget of the Antarctic Circumpolar Current in the Fine-Resolution Antarctic Model. *J. Phys. Oceanogr.*, **24**, 1201-1223.

Krupitsky, A., V. M. Kamenkovich, N. Naik and M. A. Cane, 1996: A linear equivalent barotropic model of the Antarctic Circumpolar Current in the Fine Resolution Antarctic Model. *J. Phys. Oceanogr.*, **24**, 1203-1224.

Lutjeharms, J. R. E. and A. L. Gordon, 1987: Shedding of an Agulhas ring observed at sea. *Nature*, **325**, 138-140.

Lutjeharms, J. R. E., 1988: Examples of extreme circulation events at the Agulhas retroflection. *S. Afr. J. Sci.,* **84**, 584-586.

Lutjeharms, J. R. E. and H. R. Valentine, 1988: Eddies at the subtropical convergence south of Africa. *J. Phys. Oceanogr.,* **18**, 761-774.

Lutjeharms, J. R. E. and R. C. Van Ballegooyen, 1988: Anomalous upstream retroflection in the Agulhas Current. *Science*, **240**, 1770-1772.

Manabe, S., K. Bryan, and M. J. Spelman, 1990: Transient response of a global ocean-atmosphere model to a doubling of atmospheric carbon dioxide. *J. Phys. Oceanogr.*, **20**, 722-749.

Marshall, D., 1995: Topographic steering of the Antarctic Circumpolar Current. *J. Phys. Oceanogr.*, **25**, 1636-1650.

McCartney, M. S. and M. E. Woodgate-Jones, 1991: A deep-reaching anticyclonic eddy in the subtropical gyre of the eastern South Atlantic. *Deep-Sea Res.*, **38**, S411-S443.

Munk, W. H. and A. Palmen, 1951: Note on the dynamics of the Antarctic Circumpolar Current. *Tellus*, **3**, 53-55.

Nelson, G. and L. Hutchings, 1983: The Benguela upwelling area. *Prog. Oceanogr.*, **12**, 333-356.

Nof, D., 1981: On the β-induced movement of isolated baroclinic eddies. *J. Phys. Oceanogr.,* **11**, 1662-1672.

Nof, D., 2000a: Does the wind control the import and export of the South Atlantic? *J. Phys. Oceanogr.*, **30**, 2650-2667.

Nof, D., 2000b: Why much of the circulation in the Atlantic enters the Caribbean Sea and very little of the Pacific circulation enters the Sea of Japan. *Prog. in Oceanogr.,* **45**, 39-67.

Nof, D., 2002: Is there a meridional overturning cell in the Pacific and Indian Oceans? *J. Phys. Oceanogr.*, **32**, 1947-1959.

Nowlin, W.D., and J.M. Klinck, 1986: The physics of the Antarctic Circumpolar Current. *Rev. of Geophys.*, **24**, 469-491.

Olson, D. B. and R. H. Evans, 1986. Rings of the Agulhas Current. *Deep-Sea Res.,* **33**, 27-42.

Orsi, A.H., T. Whitworth III, and W.D. Nowlin, Jr., 1995: On the meridional extent and fronts of the Antarctic Circumpolar Current, Deep-Sea Research I, 42, 641-673.

Parsons, A. T., 1969: A two-layer model of Gulf Stream separation. *J. Fluid. Mech.,* **39**, 511-528.

Pedlosky, J., L. J. Pratt, M. A. Spall and K. R. Helfrich, 1997: Circulation around islands and ridges. *J. Mar. Res.*, **55**, 1199-1251.

Peterson, R. G. and L. Stramma, 1991: Upper-level circulation in the South Atlantic Ocean. *Prog. Oceanogr.,* **26**, 1-73.

Pratt, L. and J. Pedlosky, 1998: Barotropic circulation around islands with friction. *J. Phys. Oceanogr.*, **28**, 2148-2162.

Radko, T., 1997: Theoretical studies in mesoscale jets and vortices. Ph. D. Dissertation, Florida State University, 129 pp.

Semtner, A. J. and R. M. Chervin, 1988: A simulation of the global ocean circulation with resolved eddies. *J. Geophys. Res.,* **93**, 15,502-15,522.

Shannon, L. V., 1985: The Benguela ecosystem. I. Evolution of the Benguela, physical features and processes. In: *Oceanography and marine biology. An annual review,* **23**, M. Barnes, ed., University Press, Aberdeen, 105-182.

Stevens, D. P., and V. O. Ivcheko, 1997: The zonal momentum balance in an eddy resolving general circulation model of the Southern Ocean. *Q. J. Royal Met. Soc.*, **123**(540), 929-951.

Stramma, L. and R. J. Peterson, 1990: The South Atlantic Current. *J. Phys. Oceanogr.*, **20**, 846-859.

Straub, D. N., 1993: On the transport and angular momentum balance of channel models of the Antarctic Circumpolar Current. *J. Phys. Oceanogr.*, **23**, 776-782.

Tansley, C. E. and D. P. Marshall, 2001a: Flow past a cylinder on a beta-plane, with application to Gulf Stream separation and the Antarctic Circumpolar Current. *J. Phys. Oceanogr.*, **31**, 3274-3283.

Tansley, C. E. and D. P. Marshall, 2001b: On the dynamics of wind-driven circumpolar currents. *J. Phys. Oceanogr.*, **31**, 3258-3273.

Treguier, A. M. and J. C. McWilliams, 1990: Topographic influences on wind-driven, stratified flow in a β-plane channel: An idealized model for the Antarctic Circumpolar Current. *J. Phys. Oceanogr.*, **20**, 321-343.

Van Ballegooyen, R. C., M. L. Gründlingh and J. R. E. Lutjeharms, 1994: Eddy fluxes of heat and salt from the southwest Indian Ocean into the southeast Atlantic Ocean: A case study. *J. Geophys. Res.*, **99**, 14053-14070.

Whitworth, T. III and W. D. Nowlin, Jr., 1987: Water masses and currents of the southern ocean at the Greenwich Meridian. *J. Geophys. Res.*, **92**, 6462-6476.

Zalesak, S. T., 1979: Fully multidimensional flux-corrected transport algorithms for fluids. *J. Comput. Phys.,* **31**, 335-362.